BNL-73121-2004-JA-R1

MODELING ATMOSPHERIC SULFUR OVER THE NORTHERN HEMISPHERE DURING THE ACE-2 EXPERIMENTAL PERIOD

C. M. Benkovitz[1], S. E. Schwartz[1], M. P. Jensen[2], M. A. Miller[1],
R. C. Easter[3], T. S. Bates[4]

Original Manuscript: April 2004
Revised: July 2004
Accepted: August 2004

Accepted for publication in
Journal of Geophysical Research

[1] Brookhaven National Laboratory, Upton, New York, NY 11973
[2] Columbia University, New York, NY 10027
[3] Pacific Northwest National Laboratory, Richland, WA 99352
[4] Pacific Marine Environmental Laboratory, Seattle, WA 98115

Research by BNL investigators was performed under the auspices of the U.S. Department of Energy under Contract No. DE-AC02-98CH10886.

Revised: July 1, 2004

Modeling Atmospheric Sulfur over the Northern Hemisphere During the ACE-2 Experimental Period

Carmen M. Benkovitz[1], Stephen E. Schwartz[1], Michael P. Jensen[2], Mark A. Miller[1], R.C. Easter[3], Timothy S. Bates[4]

Abstract. A high-resolution (1°×1°, 27 vertical levels) Eulerian chemical transport and transformation model for sulfate, SO_2, and related species driven by analyzed forecast meteorological data has been run for the Northern Hemisphere for June-July 1997 and extensively evaluated with observational data, mainly from air-quality and precipitation chemistry networks. For ~ 5000 evaluations, 50% of the modeled sulfate 24-h mixing ratios were within a factor of 1.85 of the observations; 50% of ~ 328 concurrent subgrid observations were within a factor of 1.33. Much greater subgrid variation for 24-h SO_2 mixing ratios (50% of ~ 3552 observations were within a factor of 2.32) reflects high variability of this primary species; for ~ 12600 evaluations 50% of modeled mixing ratios were within a factor of 2.54 of the observations. These results indicate that a substantial fraction of the modeled and observed differences is due to subgrid variation and/or measurement error. Sulfate mixing ratios are identified by source type (biogenic, volcanic, and anthropogenic) and production mechanism (primary and by gas-phase and aqueous-phase oxidation). Examination of key diagnostics showed substantial variation for the different types of sulfur, e.g., SO_2 aqueous-phase oxidation rates of 29 to 102% day^{-1}, sulfate residence times of 4 to 9 days. Volcanic emissions contributed 10% of the sulfate burden and 6% of emissions, because the elevated release allows

[1] Brookhaven National Laboratory, Upton, New York, NY 11973
[2] Columbia University, New York, NY 10027
[3] Pacific Northwest National Laboratory, Richland, WA 99352
[4] Pacific Marine Environmental Laboratory, Seattle, WA 98115

large fractional conversion of SO_2 and long residence time. Biogenic SO_2 was generally at lower concentrations than H_2O_2, resulting in efficient aqueous-phase oxidation; this source type contributed 13% of emissions but only 5% of sulfate burden. Anthropogenic sources were the dominant contributors to sulfur emissions, 80%, and sulfate burden, 84%.

1. Introduction

Atmospheric aerosols are recognized to have provided a substantial secular forcing of climate change over the industrial period, but of highly uncertain magnitude [*Ramaswamy et al.*, 2001]; therefore it is essential that aerosol radiative forcing be well quantified and accurately represented in climate models to provide a sound basis for formulating policy regarding the reduction of anthropogenic influences on climate. Representations of aerosol processes in Chemical Transport Models (CTMs) are necessary to develop and test such representations for use in climate models [*National Research Council Panel on Aerosol Radiative Forcing and Climate*, 1996]. Intercontinental transport of aerosols has been demonstrated by in-situ measurements [*Jaffe et al.*, 2003; *Prospero*, 1999; *Talbot et al.*, 1986; *Wotawa and Trainer*, 2000] and by satellite observations that have followed the plumes of smoke from forest fires over thousands of kilometers [*Heald et al.*, 2003; *Prasad et al.*, 2002; *Wooster and Strub*, 2002]; the causes and effects of events such as these can be better determined if CTMs allocate aerosol loadings by source regions, source types, and formation processes. Because of the highly nonuniform distribution of the sources of accumulation mode aerosol particles, their spatially and temporally intermittent removal, and their short atmospheric residence times, about a week, e.g. [*Cambray et al.*, 1987; *Chamberlain*, 1991], representation of the processes governing the geographical distribution of these particles in CTMs and evaluation of model performance require high space- ($\leq$ 400 km) and time- ($\leq$ 24 h) resolution [*Benkovitz et al.*, 1994].

A major component of aerosols in industrialized regions of the world is sulfate resulting from the oxidation of anthropogenic sulfur dioxide (SO_2) [*U. S. Environmental Protection Agency*, 2001]. On regional and local scales this sulfate has been linked to adverse health effects [*Vedal*, 1997], visibility impairment [*U. S. Environmental Protection Agency*, 2001], ecological damage [*Kuylenstierna et al.*, 2001], and acid rain [*Cowling*, 1982]. Sulfate has become a valuable testbed for CTMs representing aerosols for several reasons: its importance as an anthropogenic species, fairly well developed emissions inventories, emissions with rather low temporal variability, and well understood atmospheric chemistry albeit with complexities arising from production by both gas-phase and aqueous-phase reactions.

Several models that include representations of the sulfur cycle have been developed, for example [*Barth et al.*, 2000; *Chin et al.*, 2000a; *Chin et al.*, 2000b; *Koch et al.*, 1999; *Langner and Rodhe*, 1991; *Rasch et al.*, 2000a; *Roelofs et al.*, 1998], and intercomparisons of global scale model results have been conducted [*Barrie et al.*, 2001; *Lohmann et al.*, 2001; *Penner et al.*, 2001; *Rasch et al.*, 2000b; *Roelofs et al.*, 2001]. A majority of the models are General Circulation Model (GCMs) with sulfur chemistry added or are driven by meteorological data from GCMs; such models have the advantage of being able to generate statistics on monthly and annual mean concentrations. However, because sulfate concentrations are highly variable due to meteorological variability, the results from such models can be compared to observations only in rather long temporal averages and do not permit comparison with specific episodes or individual days. Thus comparison studies with such models typically report results in terms of annual or seasonal averages, with limited quantitative statistics as a consequence of the small number of samples.

Two recent intercomparison studies examined model results and attempted to account for the differences found. Comparison of the results of nine models [*Barrie et al.*, 2001] found that differences in representations of processes in the models resulted in rather large differences in the relative importance of different processes in the sulfur cycle; for example, estimates of the fraction of total sulfur removed by dry deposition in the several models ranged from 36 to 54%, residence times ranged from 3.6 to 7.5 days for sulfate, from 1.3 to 3.1 days for SO_2, and from 1 to 3.9 days for DMS. The dominant cause of model-to-model differences in regional sulfur budgets within emissions source regions was found to be the representations of in-cloud processes: aqueous-phase oxidation, wet deposition, and vertical transport; outside the source regions the efficiency of horizontal transport is also of importance. In spite of such differences most models predicted surface seasonal mean sulfate MRs within 20%; this suggests the need for finer spatial and temporal resolution in the comparison of model results with observations, and more detailed examination of how the differences in process representations interact, perhaps via compensating errors, to produce similar results. The results of eleven models were examined at a series of remote surface stations by Penner et al. [2001]; the envelope of the modeled annual average sulfate concentrations was between 0.1 and 3 μg^{-3}, and excluding model results that were considered outliers based on their comparisons with observations, the spread of the estimated sulfate aerosol burden was a factor of 2.2. There is thus a great need to understand these differences between models; both studies recommended more detailed measurements, especially in remote areas and in the vertical, against which to test model parameterizations of aerosol processes as well as model results.

The work reported here is a study conducted using the Global Chemistry Model driven by Observation-derived meteorology (GChM-O), an Eulerian CTM that represents the sulfur

cycle and calculates distributions of sulfate, SO_2, dimethyl sulfide (DMS), and methanesulfonic acid (MSA) with high spatial and temporal resolution, for specific times and locations, by source region, source type, and sulfate formation process. A previous study reported results from calculations using an earlier version of this model and extensive comparisons with observations in simulations of four seasonal 6-week periods in 1986-1987 [*Benkovitz et al.*, 1994; *Benkovitz and Schwartz*, 1997]. Because the model was driven by analyzed forecast meteorological data it was possible to obtain extensive evaluation of model results and observed mixing ratios (MRs) for short periods of time (typically 24 h as governed by measurement protocols) and at numerous locations. Benkovitz and Schwartz [1997] reported approximately 8000 model observation evaluations for sulfate and approximately 20000 evaluations for SO_2; a large fraction of the departure between modeled and observed MRs was attributed to subgrid variability and/or nonrepresentative sampling of model grid cells at the stations used for the evaluations.

The present version of the model includes refined parameterizations of chemical mechanisms, aerosol uptake by clouds, and wet removal. In the previous sub-hemispheric model (140°W to 60°E longitude) much of the sulfate aerosol was exported from the modeling domain; therefore, the domain of the current model has been expanded to include the Northern Hemisphere from the equator to 81°N. This expanded domain incorporates all industrialized areas of the hemisphere and allows examination of the influence of the several major source regions. This version of the model has been used to simulate the period of the Aerosol Characterization Experiment-2 (ACE-2), which took place in June-July 1997 over the eastern North Atlantic [*Raes et al.*, 2000].

Measurements conducted as part of ACE-2 obtained high space- and time-resolution observations of the concentrations of aerosols and precursor species; measurements taken at

Tenerife, Canary Islands and at Sagres, Portugal permitted a case study of results of the model simulation in this region [*Benkovitz et al.*, 2003]. Detailed evaluations of the simulation results demonstrated that the model was capable of representing sulfate MRs at Tenerife (minimal influence from proximate sources) within the inter-measurement and subgrid variations. At Sagres (influenced by proximate sources) the spread between model and observations was larger; this was attributed to the nonrepresentativeness of a single measurement at a location where considerable subgrid variation can be expected. Although Tenerife is geographically much closer to Europe than to North America, the contributions from European, North American, and biogenic sources to the sulfate burden in this time period were comparable at this location, with North American sources dominating (up to ~ 85%) under conditions of a strong Azores high.

The work described here extends the evaluation of model results using observations from routine air quality monitoring stations in North America, Europe, and Taiwan, and stations in the Canary Islands and Korea. Measures of rates and extent of important processes (yields, conversion, removal rates, etc.) calculated from model results are reported, permitting comparison of these quantities as represented in other models.

2. Description of the Model

The model used in this study is a three-dimensional Eulerian transport and transformation model for sulfate, MSA, and precursor species. Species abundance is reported as mixing ratio (MR, mol per mol air; 1 nmol mol^{-1} = 1 ppb), as this quantity is invariant to expansion and compression due to fluctuations in pressure and temperature. The model represents emissions of SO_2 and DMS, transport, convective mixing, conversion of SO_2 to sulfate by H_2O_2 and O_3 in the aqueous phase and by OH in the gas phase, gas-phase conversion of DMS to SO_2 and MSA by

OH, wet removal, and dry deposition. The model domain includes the entire Northern Hemisphere from the equator to 81°N, and because this domain is not global, it is necessary to account for material advected into the model domain by assigning representative background concentrations; this external material is carried as separate variables. The model is initialized with the mixing ratio of all species set to zero. The processes represented in GChM-O Version 2 are outlined in Figure 1, the chemical species represented in the model are defined in Table 1 and the model input data and their provenance are summarized in Table 2. The earlier version of the model was described in Benkovitz et al. [1994]; changes in Version 2 are described here.

2.1. Meteorological Data

The meteorological data used were obtained from the European Centre for Medium-Range Weather Forecasts (ECMWF) [*European Centre for Medium-Range Weather Forecasts*, 2003]. Quantities used were the 6-h instantaneous values from the initialized analysis surface fields (2-D) and model-level fields (3D) except for precipitation, heat fluxes, and thermal radiation, which were the accumulated 6-h values from the gridded 12, 18, 24, and 30 hour forecasts at the same resolution. The effects of the ECMWF model spinup on the precipitation, heat fluxes, and thermal radiation values were minimized by using the 12UT daily forecasts and adding the forecast hour to the date to find the new date; for example, values from the 12, 18, 24, and 30 hour forecasts on June 6 at 12UT were used for June 7 at 00UT, 06UT, 12UT, and 18UT (K. Fielding, European Centre for Medium-Range Weather Forecasts, personal communication, 1999). For the simulations reported here the model domain extends from 0° to 360° longitude and from the equator to 81°N with 1° resolution (approximately 111 × 111 km at the equator and 56 × 111 km at 60° latitude) and 27 levels from the surface to ~ 100 hPa.

2.1.1 Height of the mixed layer

Estimates of the height of the mixed layer were required to set the vertical diffusivity coefficient; these estimates must account for differences over land and ocean areas and for the diurnal cycle of this parameter. In Version 1 the mixed layer heights had been set to a constant seasonal value; in Version 2 time- and location-dependent mixed layer heights were calculated by a multi-step approach based on the equivalent potential temperature (θ_e), the saturation equivalent potential temperature, (θ_{es}), the dew point, (T_d), and the height (above ground) of the model vertical levels as detailed in Appendix A. The algorithm developed captures the major global features expected in the mixed layer height (Figure 2), such as a general increase in height over the oceans from the poles to the tropics, relatively lower height over regions of ocean upwelling such as off the coast of California, and a clear diurnal cycle, particularly over land.

2.1.2 Vertical diffusivity coefficient

The default value for the vertical diffusivity coefficient K_{zz} was set to 10 m^2 s^{-1} [*Ko and Sze*, 1991; *Louis*, 1979; *Pasquill*, 1976]. If the value of the K number, defined as $K = K_{zz}\,\Delta t/(\Delta z)^2$ [*Brasseur and Madronich*, 1992] where Δt is the transport time step and Δz is the thickness of the model level, was greater than 0.5 the value of K_{zz} was adjusted so that the K number was less than or equal to 0.5. Above the mixed layer vertical diffusion was assumed to be negligible compared to other transport processes so values of K_{zz} were set to zero.

2.2 Chemistry

2.2.1 Chemical mechanisms

The model represents aqueous-phase oxidation of SO_2 to sulfate by H_2O_2 and O_3, OH-induced gas-phase oxidation of SO_2 to sulfate and of DMS to SO_2 and MSA, and gas-phase production of H_2O_2 from HO_2. Version 1 of the model incorporated all the sulfate present into

cloud water and used the limiting reagent formulation for the reaction of SO_2 with H_2O_2; in the current version the incorporation of sulfate into cloud water and the extent of aqueous phase oxidation of SO_2 are explicitly calculated.

Aqueous-phase oxidation is calculated for all clouds for which the liquid water volume fraction (LWVF) was equal to or greater than 10^{-9}. The fraction of sulfate that is in the aqueous phase (i.e., cloud drops) is important for both the cloud water pH and the sulfate wet removal. Subgrid variability of clouds was accounted for by incorporating the sulfate into cloud water according to the LWVF as follows:

$$f_r = \frac{f_{max}\left(\frac{L}{L_{mid}}\right)}{1+\frac{L}{L_{mid}}}$$

where f_r is the fraction of sulfate aerosol that is incorporated into cloud water, f_{max} is the maximum fraction of sulfate that is incorporated into cloud water, L is the grid-cell averaged liquid water volume fraction, and L_{mid} was the liquid water volume fraction corresponding to $0.5f_{max}$. A value of 0.5 was used for f_{max} based on ten Brink et al. [1987], Daum et al. [1984], and Leaitch et al. [1983], who examined aircraft measurements of the composition of cloud liquid water, interstitial air, and associated clear air to estimate the fraction of unscavenged sulfate aerosol. A value of 10^{-7} was used for L_{mid}; the resulting uptake function is shown in Figure 3. Cloud-water pH was estimated assuming that sulfate was present entirely as ammonium bisulfate and that MSA was fully dissociated; pH was constrained to be between 2.0 and 5.6. Kinetics of the aqueous-phase oxidation of SO_2 by H_2O_2 and O_3 were explicitly represented. Expressions for the temperature- and pH-dependent Henry's law coefficients and dissociation constants for the

absorption of gaseous SO_2 in water were taken from Goldberg & Parker [1985]. Expressions for the temperature-dependent Henry's law coefficient of H_2O_2 and O_3 are taken from Easter [1988]. For the oxidation by H_2O_2 the second-order expression is taken from Schwartz [1988], based on Overton [1985]. For the oxidation by O_3 the second order expression is taken from Schwartz [1988], who used the rate coefficients of Hoigné et al. [1985] with temperature adjustments from Erickson et al. [1977].

2.2.2 Oxidant mixing ratios.

Mixing ratios of oxidant species HO_2, H_2O_2, O_3 and OH were based on monthly average MRs for June and July calculated using Version 2 of the Model of Ozone and Related Chemical Tracers, (MOZART) [*Brasseur et al.*, 1998; *Horowitz et al.*, 2003] driven by a GCM, the NCAR Community Climate Model. MOZART is a global model with 2.8° resolution in longitude and latitude and 25 vertical levels from 992 to 5 hPa. Anthropogenic emissions used in the MOZART simulation were taken from the EDGAR Version 2 inventory [*Olivier et al.*, 1996], which represents emissions ca. 1990, with some modifications based on preliminary values from the EDGAR Version 3 inventory [*Olivier and Berdowski*, 2001]; biogenic emissions were based on the work of Guenther et al. [1995], Müller [1992], and Yienger and Levy [1995]; oceanic emissions were modified values from the inventory by Brasseur et al. [*Brasseur et al.*, 1998]; lightning emissions were based on the parameterizations of Price et al. [*Price et al.*, 1997] and Pickering et al. [1998].

As the daily average MRs generated by MOZART were obtained using a CTM driven by a GCM, the oxidant MRs are representative of typical conditions as opposed to specific meteorological situations. The day-to-day variability in the MOZART oxidant MRs was eliminated, but the geographic distribution preserved, by averaging the MRs over the June-July

modeling period at each location and level of the MOZART model. The resulting averages exhibited somewhat high OH MRs over the continents, with maxima of about 6×10^6 cm^{-3}. The grid-to-grid conversion was performed as follows. Each horizontal GChM-O grid cell was located within the larger MOZART grid, followed by linear interpolation between the lowest and highest MOZART vertical levels to the GChM-O vertical levels. The value of the lowest MOZART level was used for all the GChM-O levels within the lowest MOZART level. The hourly MRs for HO_2 and OH were obtained as the product of the average values and the cosine of the solar zenith angle for each location and time.

H_2O_2 is included in the model as an advected species formed by the reaction $2HO_2 \rightarrow H_2O_2 + (O_2)$; the values of the rate constant for this reaction were taken from Stockwell [1995] and NASA [1997]. H_2O_2 is removed by aqueous-phase oxidation of SO_2 and by wet and dry deposition; because sinks of H_2O_2 via photolysis, reaction with OH, and below cloud scavenging were not explicitly represented, these were taken into account by not allowing the H_2O_2 MRs to exceed values obtained by the MOZART model.

2.3 Wet Removal

Wet removal of sulfate and MSA incorporated in cloud water was represented by an exponential function:

$$f_k = e^{-\frac{P\,\Delta t}{B}\frac{W_k}{W_{\max}}}$$

where f_k is the fraction of aerosol remaining in the aqueous phase at vertical level k after model time step Δt (s), P is the precipitation rate at the surface (mol m^{-2} s^{-1}), B is the total column cloud liquid water content (LWC, mol m^{-2}), W_k is the cloud LWC at vertical level k, and $W_{\max}$ is the

maximum cloud LWC in the column. The factor W_k/W_{max} accounts for the greater rate of precipitation formation at higher cloud LWC.

2.4 Emissions

2.4.1 Anthropogenic emissions of SO_2 and primary sulfate.

Anthropogenic emissions of SO_2 were taken from the Emission Database for Global Atmospheric Research (EDGAR) Version 3.2 [*Olivier et al.*, 2002] inventory, which represents annual emissions ca. year 1995. Seasonal emissions and breakdown between release points below and above 100 m were calculated using the appropriate fractions from the GEIA Version 1B inventory [*Benkovitz et al.*, 1996]; emissions for the Northern Hemisphere summer were used. Primary sulfate emissions for 1997 were estimated by extrapolation from the GEIA inventory as 1% of the sulfur emissions for industrialized regions (North America, Europe) and 2% for the rest of the model domain. Vertically resolved SO_2 emissions from aircraft have not yet been developed for EDGAR V3.2, so the vertically-resolved aircraft emissions from EDGAR V2, which were representative of ca. 1990, were adjusted according to the ratio of the total global emissions of the Version 3.2 and Version 2 inventories (J.G.J. Olivier, National Institute for Public Health and the Environment, RIVM, personal communication, 2003). Aircraft emissions were assigned to the appropriate GChM-O vertical level and were assumed to have no seasonal pattern. Anthropogenic emissions, assumed to be constant over the simulation period, are presented in Figure 4a. A logarithmic scale of over three orders of magnitude is used to encompass the wide range of emissions density. Anthropogenic emissions were divided into three main geographic regions and the sulfate and SO_2 MRs were tracked separately for each region. The areas of high anthropogenic emissions in North America (190° to 330°, 21.1% of anthropogenic emissions), Europe (330° to 60°, 33.3% of anthropogenic emissions), and Asia

(60° to 190°, 45.6% of anthropogenic emissions) are evident in the figure; emissions over the oceans originate from ships and aircraft.

2.4.2 Biogenic emissions.

Sea surface DMS concentrations from Kettle et al.[1999] were combined with seawater DMS measurements made during the ACE-2 field campaign to calculate time- and location-dependent oceanic DMS emissions using the wind speed transfer velocity relationship of Liss and Merlivat [1986], as described in Appendix B. Seasonal emissions of DMS and H_2S from land sources were calculated using the methodology of Lamb [*Bates et al.*, 1992] gridded to 1° × 1° resolution [*Benkovitz et al.*, 1994]; these emissions were treated entirely as DMS in the model. Average biogenic emissions are presented in Figure 4b. Overall, biogenic emissions were significantly smaller and much more uniform spatially than anthropogenic emissions, with emissions from the ocean predominating. The high productivity areas in the North Atlantic south of Greenland and in the tropics south of 30°N are evident in Figure 4b.

2.4.3. Volcanic emissions.

Volcanic emissions are quite variable temporally and there were substantial volcanic events during the modeling period, so as far as possible daily sulfur emissions from volcanos were specific to the simulation period. The principal sources of time-specific information were the Volcano Activity Reports compiled by the Global Volcanism Program of the Smithsonian Institution and available at web site **http://www.volcano.si.edu/gvp/gvn/index.htm** (accessed in spring 1999) and personal communication with the principal investigators conducting measurements at individual volcanos (Table 3). As most measurement schedules were not daily, daily emissions were estimated using linear interpolation (P. Francis, Open University, personal communication, 1998). In the absence of specific information for continuously degassing

volcanos, the 25-year average emission rates from Andres and Kasgnoc [1998] were used. In the model volcanic emissions were treated entirely as SO_2.

Because emissions from Karumsky (Kamchatkan Peninsula), Satsuma Iwojima (Kikai, Japan), and Vulcano (Italy) were obtained as minimum and maximum values for periods of several days, daily emissions were estimated using a random function within the given minimum, maximum range. No information was available on the status of Apoyo (Nicaragua), Concepción (Nicaragua), and Hakkoda (Japan) so emissions from these volcanos were taken as zero. None of the active volcanos was located within the ACE-2 experimental area; the closest volcanos were Etna in Sicily and Stromboli and Vulcano in the Aeolian (Lipari) Islands at distances of ~ 2900 km.

The model injects emissions from volcanos into the atmosphere starting at the height of the cone of each volcano and extending up to four additional levels, depending on the amount of the emissions at a particular time period. At each level the fraction of the emissions injected was taken as proportional to the density of air at that level. The two largest volcano emitters during the modeling period were Popocatépetl near Mexico City and Etna in Sicily. Approximately 30% of the volcano emissions were released at heights less than 2000 m, ~ 26% between 2000 and 4000 m, and ~ 44% over 4000 m. Only three volcanos account for the emissions released at heights greater than 4000 m: Popocatépetl (Mexico, 5465 m), Ruiz (Colombia, 5321 m), and Galeras (Columbia, 4276 m).

Approximately 59% of the sulfur emissions from volcanos were based on measurements combined with interpolations, 38% were 25-yr averages assumed constant for the simulation period and 3% were based on information on minimum/maximum emissions. Information on

the volcanos active during the experimental period is presented in Table 3, and average emissions for the simulation period are presented in Figure 4c.

2.4.4. Assessment of emissions values.

Sulfur emissions in the model domain were dominated by anthropogenic sources; these sources contributed ~ 80% of the sulfur emissions, biogenic sources contributed ~ 13%, and volcanos contributed ~ 6%. The distribution of emissions by source region and source type for the 8-week simulation period and extended to one year is presented in Table 4; Asian sources were the largest contributors to both the total and the anthropogenic emissions.

As 1995 anthropogenic emissions were used in a 1997 simulation, the impact of this was assessed using information obtained from regional agencies in Europe and North America. In Europe, emissions data are reported by participants to the Convention on Long-Range Transboundary Air Pollution (CLRTAP) to the United Nations Economic Commission for Europe/Co-operative Programme for Monitoring and Evaluation of Long Range Transmission of Air Pollutants in Europe (UNECE/EMEP); in addition, expert estimates by the Meteorological Synthesizing Centre - West (MSC-W) of EMEP are also developed to supplement the reported data and for use in EMEP modeling work [*Vestreng and Klein*, 2002]. Total emissions of SO_2 in the EMEP European domain were estimated to be 16.3 Tg S in 1995 and 14.4 Tg S in 1997, ~ 12% decrease; the largest reductions were in Germany and the United Kingdom. In the United States the U.S. Environmental Protection Agency estimates yearly emissions using a "bottom-up" methodology [*U.S Environmental Protection Agency*, 2000]. The difference between emissions in 1995 and 1997 was calculated using emissions by state obtained from the U.S. Environmental Protection web site Tier Emissions Report - Criteria Air Pollutants

http://www.epa.gov/air/data/nettier.html?us~usa~United%20States . Total emissions of SO_2 in the U.S. were estimated to be 8.6 Tg S in 1995 and 8.8 Tg S in 1997, ~ 1.5% increase.

In Asia sulfur emissions have been increasing in the 1990s and estimates have larger uncertainty because of poorly developed regional emission factors and lack of accurate knowledge of the sulfur contents of the fuels used. Streets et al. [2000; 2001] estimated SO_2 emissions in Asia to be 19.2 Tg S in 1995 and 19.6 Tg S in 1997, ~ 2% increase. The country-based estimates developed by different investigators agreed to between 15% and 20% [*Benkovitz et al.*, 2004], and regional estimates agreed to ~ 4%, except for the EDGAR estimate of the Asian total which is ~ 28% higher than estimates from regional investigators.

Because most anthropogenic emissions were due to the combustion of fossil fuels, a relatively small uncertainty of ±30% had been placed on the global annual average [*Lelieveld et al.*, 1997]; however, this uncertainty increases when the combustion of biofuels and biomass burning are included in anthropogenic emissions totals. Currently no reliable new quantitative values of the uncertainty are available, although these values are thought to be well in excess of the 1995 to 1997 differences in the inventories for the several source regions.

Although the error in the annual global mean oceanic DMS surface concentrations has been estimated at ±50% [*Penner et al.*, 2001], the error in the seasonal and regional concentrations can be up to a factor of 5; these errors are compounded by differences in air/sea flux parameterizations, which can in turn add a factor of 2 difference to the estimates of DMS emissions from the ocean [*Kettle and Andreae*, 2000]. However, at locations where biogenic emissions are much smaller than anthropogenic emissions, the uncertainty in the biogenic emissions would not be a large input to the uncertainty in the total emissions.

Total volcanic sulfur emissions for the 8-week simulation period were 0.75 Tg, which corresponds to annual emissions of ~ 4.5 Tg. This estimate is comparable to the global estimates for continuous emissions presented in Table 1b of Mather et al. [2003], ~ 3 to ~ 5 Tg y^{-1}, the global estimate of 3.5 Tg S yr^{-1} for non-eruptive volcanos by Spiro et al. [1992], and the estimate of 10 Tg yr^{-1} in the Northern Hemisphere by Graf et al. [1997]. Differences in these estimates can be accounted for by the methodologies used to estimate the emissions, by the different domains covered in some of the estimates, by the intermittent nature and great discrepancies in the estimates of emissions from both degassing and eruptive events, and because measurement values used in this study were selected to represent, as much as a possible, the time period of the simulation.

3. Observations

Model results were evaluated using measurements taken during the simulation period, mainly by monitoring networks; summary information on the networks and measurements is presented in Table 5. The spatial area used for evaluation is a model grid cell (1° × 1°), referred to as a location, and model vertical level. Stations were assigned to a location based on their latitude and longitude; for each observation the model vertical level was selected according to the station altutude and the height of the model levels at the time of observation. Where concurrent measurements were available at multiple stations within a location, these were averaged to obtain the observed MRs; each pair of modeled and observed MRs at a location, vertical level, and date is referred to as a case. Concurrent observations at a location and vertical level permitted examination of intra-location variability due to subgrid variability and/or measurement error.

Sulfate and SO_2 measurements used were made by routine air quality monitoring networks in North America, Europe, and Taiwan and stations in the Canary Islands and Korea. If necessary, reported concentrations were converted from the original units to MRs in units of ppb; observations reported at station temperature and pressure were converted to MRs using the ECMWF meteorological data. Sampling start and stop times based on local time were converted to Universal Time (UT) to permit comparisons with modeled MRs. Observed MRs corrected for sea salt sulfate were used in these evaluations. A summary of the data sets is presented in Appendix C; maps of the evaluation locations are presented in Figure 5.

4. Evaluation of Model Results and Observations

A general concern with the accuracy of results obtained with CTMs driven by analyzed meteorological fields is the accuracy of values of these fields; any inaccuracy in transport parameters or in cloud and precipitation amounts and/or locations directly influences the model results. Thus even if all the aerosol processes were accurately represented in the model, errors in the meteorological fields would degrade the evaluations between modeled and observed values; consequently any departure reflects inaccuracy both in the representation of the processes in the model and in the meteorological fields that drive the CTM. Especially important are the three-dimensional field of cloud presence and the two-dimensional fields of cloud fraction and precipitation amount, which are difficult to accurately represent in numerical weather prediction models [*Jung and Tompkins*, 2003; *Mullen and Buizza*, 2001]. In the present model the non-reanalyzed 1997 ECMWF data were used; these forecasts overestimated the precipitation amount, although subsequent changes in the model resolution and physical parameterizations starting in 1999 have gone a long way towards correcting the overestimation [*Cherubini et al.*, 2001; *Lalaurette et al.*, 2003]. Errors in these fields directly influence both the principal

mechanism of sulfate formation, aqueous-phase conversion of SO_2 to sulfate, and the principal sink of aerosol sulfate, wet deposition. In addition, any errors in wind speed and direction and/or times, locations and amounts of cloud and precipitation fields result in temporal and spatial displacements of modeled values with respect to the observations, which degrade point-to-point evaluations. If such displacements could be taken into account evaluation results would improve, and examination of residual errors might refine understanding of representation of chemical and scavenging processes. These considerations suggest the utility of additional tools, such as visualization and pattern recognition techniques, to enhance the utility of model-observation evaluations. An initial step in this direction, taken here, is comparison of time series at specific locations, in which temporal displacement becomes readily apparent.

4.1 Time series of sulfate and SO_2 Mixing Ratios

Time series of the modeled and observed sulfate MRs at all 90 locations for which sulfate was measured on at least 28 of the 38 analysis days are shown in Figure 6. The model accurately reflected the spatial distribution of sulfate; in general locations with small observed MRs exhibited small modeled MRs and vice versa. In addition, almost all locations displayed good agreement in episodicity (patterns of short-term temporal variability) and quite a few displayed good agreement in magnitude, with locations in source regions exhibiting the greatest discrepancies in magnitude and sometimes in episodicity. There were several instances of remarkably good quantitative agreement, for example, locations in Norway (8,58,0), Denmark (10,54,0), Sweden (17,58,0), Great Britain (353,54,0), and Spain (358,42,0); the notation by which the locations are labeled is explained in Figure 7. Examples of agreement in epidisodicity, but not as good agreement in magnitude, were locations in Slovakia (19,49,2) and Canada (282,46,0) and (294,44,0). Examples of temporal displacement of modeled values were

locations in Poland (17,54,0) and Latvia (21,56,0). Locations (8,58,0), (10,54,0), (21,56,0), and (17,58,0) were in northern Europe, in areas not impacted directly by SO_2 emissions from central Europe; locations (353,54,0), and (358,42,0) were in western Europe upwind from areas of high SO_2 emissions. Locations (17,54,0) and (19,49,2) were in areas of high SO_2 emissions in central Europe; locations (282,46,0) and (294,44,0) were downwind from areas of high emissions in North America.

The high temporal and spatial variability of SO_2 lead to mixed results in the time series analysis. Figure 7 presents SO_2 time series at four of the 274 locations available for this analysis. At a location in Taiwan (120,22) the modeled MRs were within the scatter of the observed MRs; however, the model mostly overestimated the average MRs. Another location in Taiwan (120,24) presents an example of extreme spatial inhomogeneity; the single station with high observed MRs sufficiently influenced the average observed MRs that model results substantially underestimated the average MRs. A location in Georgia, USA (269,38) presents an example of good agreement between modeled and average observed MRs and a location in New Hampshire, USA (287,43) presents an example of the consequences of setting an artificial lower limit to reported quantities.

4.2 Quantitative evaluation of sulfate and SO_2 mixing ratios

In over half the cases (~ 56%) modeled sulfate MRs were within a factor of 2 of the observed MRs, and ~ 77% of the modeled MRs were within a factor of 3 (Figure 8a). The distribution of modeled and observed values is almost symmetrical below and above the 1:1 line; for example, MR_m/MR_o was between 1 and 2 in 27.0% of the cases and between 0.5 and 1 in 28.5% of the cases, with similar results for the other ranges. SO_2 modeled and observed MRs exhibited somewhat greater departure (Figure 8b) with ~ 39% of the ratios within a factor of 2

and ~ 56% within a factor of 3, and the distribution of the ratios of modeled to observed values was skewed towards values greater than 1. For MRs averaged over the whole 38-day simulation (similar to monthly averages commonly reported), the factor of 2 and factor of 3 percentages increased to 65.3% and 90.0% for sulfate and to 45.5% and 59.8% for SO_2; the improved agreement between model values and averaged observations illustrates how model evaluations using longer time periods tend to smooth over differences between modeled and observed values. As model errors may be masked by the longer averaging period, a more stringent evaluation of model performance is obtained by comparisons at fine temporal resolution.

The model performance was quantitatively evaluated by examination of the differences between modeled and observed MRs and the ratio characteristic spread. Histograms of MR_m - MR_o, classified by the observed value (Figure 9), permit assessment of model bias. For both sulfate and SO_2 the distributions peaked at a low value of this difference and were reasonably symmetric about zero, indicative of a lack of bias of the model. As the peaks in the distributions include a wide range of observed MRs, not just small values, the model accuracy indicated by the histogram is not just a consequence of small differences when observed MRs are small. Approximately 52% of the sulfate observations and ~ 59% of the SO_2 observations were overestimated by the model.

The ratio characteristic spread (S) used in this work is a measure of the ratios of MRs [*Benkovitz and Schwartz*, 1997]. A study by McNair et al. [1996] concluded that the spatial variability in observed pollutant concentrations within model grid cells should be taken into account in developing performance guidelines for model evaluation. For evaluation of two observed MRs, $S_{o/o}$, or for evaluation of modeled and observed MR, $S_{m/o}$, S is defined as the ratio of the greater MR to the lesser MR. For more than two observed MRs this definition is

generalized as $S_{o/o} = \exp[2\text{s.d.}(\ln MR_o)]$ and $S_{m/o} = \exp[|\ln(MR_m / \overline{MR_o})|]$, where MR_o is the observed MR, MR_m is the modeled MR, s.d. is the standard deviation, and $\overline{MR_o}$ is the average of the observed MRs. As a measure of the spread of the observed MRs due to analytical uncertainties, different measurement techniques, sampling protocols, and/or subgrid variation, the spread of multiple observations within a single grid cell for a single observation period, $S_{o/o}$, is a measure of the best agreement that might be expected between modeled and observed MRs. Thus multiple observed MRs at different sites within individual model grid cells are needed to assess the expected agreement.

For sulfate the distributions of $S_{o/o}$ and $S_{m/o}$ for the multiple observations set (Figure 10a and b) were similar, but somewhat broader for $S_{m/o}$, with median values of 1.33 for $S_{o/o}$ and 1.66 for $S_{m/o}$. The relative contribution of each observed MR range to each range of S was similar between the two distributions, with comparable fractions exhibiting values of S greater than 5. Of the 1.66 value of $S_{m/o}$ 1.33 was attributed to subgrid variation and/or measurement error and a comparable amount was attributed to model error. The distribution of $S_{m/o}$ for the entire data set (Figure 10c) was broader than for the multiple observations set, with a median value of 1.85 and a greater fraction of the cases with $S_{m/o}$ values greater than 5. The relative contributions of each observed MR range to each $S_{m/o}$ range were impacted mainly by the differences in the relative fractions of cases where the observed MRs were less than 0.33 ppb and greater than 3 ppb. The larger value of $S_{m/o}$ for the entire data set may be due to subgrid variability not being captured by a single monitoring station, and/or to greater measurement or model error at smaller MRs.

For SO_2 the distribution of $S_{o/o}$ (Figure 10d) is broader than that of $S_{m/o}$ (Figure 10e), with median values of 2.32 and 1.87 respectively. Measured SO_2 MRs can have great temporal and spatial variability within individual locations, as shown in Benkovitz et al. [1997] and in Figure 7; the narrower distribution and smaller median value of $S_{m/o}$ compared to $S_{o/o}$ could be a result of averaging the measurements to obtain the observed MRs used in the model evaluation. The relative contribution of each observation range to each category was similar between the two distributions, and the fraction of the evaluations with S values greater than 8 is approximately the same for both. The median value of $S_{m/o}$ for the entire data set was 2.55, a large fraction attributable to the high degree of within-location spatial variation evident from the median value of $S_{o/o}$. The distribution of $S_{m/o}$ (Figure 10f) was similar to but broader than that of $S_{m/o}$ for the multiple observations set, with the relative contributions of each observed MR range to each $S_{m/o}$ range impacted mainly by the differences in the relative fractions of cases where the observed MRs were less than 1 ppb. Values of $S_{m/o}$ exceeded 8 in approximately 17% of the evaluations; of these approximately 1.4% were from locations for which more than 50% of the $S_{m/o}$ values were greater than 8, but only ~ 16% of the locations with larger discrepancies had multiple observations. Locations with more than 50% of their $S_{m/o}$ values greater than 8 were in the larger emissions areas of central and eastern Europe, where most of the modeled MRs were overestimated (possibly because of overestimated SO_2 emissions), and a few locations in western North America where most of the modeled MRs were underestimated, possibly because of subgrid variability not being appropriately captured or because of spatial and/or temporal displacement errors.

4.3 Quantitative evaluation of sulfate concentration in precipitation

In contrast to sulfate MRs, for which little model bias was exhibited, there was considerable bias in the modeled concentrations of sulfate in precipitation, with ~ 74% of the observed concentrations overestimated by the model. All of the observed concentrations less than 5 μmol L^{-1} were overestimated, and ~ 34% of the observed concentrations in the range of 10 to 20 μmol L^{-1} were overestimated (Figure 9c). Approximately 45% of the modeled concentrations were within 10 μmol L^{-1} of the observed concentrations, and ~ 27% of the differences between modeled and observed concentrations were greater than 40 μmol L^{-1}.

For the observed sulfate concentration in precipitation approximately 29% of the concurrent measurements locations had stations separated by 10 km or less with a median distance of ~ 40 km; this may account for the high percentage of $S_{o/o}$ values less than or equal to 1.5 (Figure 10g). For the multiple observation data set the distribution $S_{o/o}$ was much narrower than that of $S_{m/o}$ (Figure 10g and h), with median values of 1.36 and 2.44 respectively. Values of $S_{o/o}$ exceeded 6 only for observed concentrations in the 10 to 20 μmol L^{-1} range, whereas the $S_{m/o}$ values greater than 6 included observations from all ranges. The median value of $S_{m/o}$ for the whole data set was 2.82 (Figure 10i), slightly higher than that for the multiple data set, with ~ 17% of the cases having $S_{m/o}$ values greater than 8; of these ~ 8.5% were from locations that had more than 50% of the $S_{m/o}$ values greater than 8, but only ~ 18% of the locations with large discrepancies had multiple observations (usually two stations). Only two locations with $S_{m/o}$ values greater than 8 were located in Europe and in both the concentrations were underestimated; the rest of the locations were in North America where most of the concentrations were overestimated in areas with large emissions (eastern half, larger

precipitation) and underestimated in areas with smaller emissions (western half, smaller precipitation).

Analyses of concurrent observations within a model grid cell ($S_{o/o}$) and of the modeled and observed MRs ($S_{m/o}$) with fine temporal resolution demonstrate that the model represents the observed sulfate and SO_2 MRs with an accuracy comparable to the spatial variability and measurement error of the observed MRs. These analyses demonstrate the need for concurrent multiple measurements at locations where substantial subgrid variability is expected (for example, those within or close to major emissions regions) to adequately capture this variability and thus allow more accurate evaluations of model results. These analyses also demonstrate the importance of driving the model with meteorological quantities and other model input data representing as accurately as possible the conditions at the time when the observations were made.

5. Discussion

Quantities such as contributions of source regions to emissions and to sulfate burdens, turnover times (mean residence time, τ) and removal rates (inverse τ, τ^{-1}) for both sulfate and SO_2, and the yields for aerosol sulfate and MSA are some of the measures of the performance of a model which may be compared to other estimates of these quantities, and which can be used in simpler models and for studies such as those that estimate sulfate radiative forcing [*Charlson et al.*, 1992; *Haywood and Shine*, 1995]. Despite the fact that the present model may not represent a "steady state" system, and the geographic domain was not completely "closed", nonetheless it is possible to estimate these key budget quantities based on the model results. Material flowed out of the south, north and the top boundaries of the model domain, although transport across the equator is known to be slow in comparison with removal rates, and MRs at the northern and top

boundaries were small. For the 6-week analysis period the sulfate outflow (flow out of the domain) averaged between ~ 2% of the total sinks for North American sources and ~ 5% for volcanic sources; SO_2 outflow averaged less than 1% except for volcanic sources for which it was less than 2%. Volcanic sources have the most outflow because the largest emitting volcano, Popocatépetl, is located near the southern border of the model domain. Sulfate formed in the aqueous phase and deposited in the same event did not contribute to atmospheric aerosol sulfate; therefore, these amounts were not included in calculations of aerosol sulfate yields and turnover times. As discussed in Benkovitz et al. [1994] the following calculations were based on burdens and sink rates. For sulfate and MSA sinks were wet and dry deposition; for SO_2 sinks were chemical conversion, and wet and dry deposition. Estimates of turnover times and removal rates for any given species were calculated as $\tau = \int B\mathrm{d}t / \int S\mathrm{d}t$, where B is the burden (mol) and S is the sink rate (mol h^{-1}) in the domain integrated over the analysis period; the sink rate does not include the outflow material. The sulfate and MSA yields were calculated as $y = \int C\mathrm{d}t / \int S\mathrm{d}t$ where C is the chemical conversion rate of SO_2 to sulfate or DMS to MSA (mol h^{-1}) respectively in the domain integrated over the analysis period.

Aqueous-phase oxidation of SO_2 by H_2O_2 is the principal mechanism for the generation of sulfate. Therefore, for each source region and source type the fraction of SO_2 in areas where the SO_2 MR was less than the H_2O_2 MR and the fraction of SO_2 that encountered clouds are key factors in the relative importance of sulfate generation mechanisms and of the SO_2 sinks. The domain-average fraction of SO_2 located in areas where the SO_2 MR was less than the H_2O_2 MR was calculated as

$$\overline{F_{SO_2}} = \frac{\sum_{i,j} A \sum_{k} f \, c_{SO_2} \Delta h_k}{\sum_{i,j} A \sum_{k} c_{SO_2} \Delta h_k}$$

where A is the area of the grid cell (m^2), f is equal to one if the SO_2 MR is less than the H_2O_2 MR and equal to zero otherwise, c is the SO_2 concentration (mol m^{-3}), and Δh_k is the depth of model level k (m). The SO_2 MR was greater than the H_2O_2 MR mainly over large anthropogenic source areas (Figure 11). These areas extended to higher model levels over Europe and Central Asia because ~ 49% of the emissions from European sources were emitted into the second model level, as compared to ~ 39% for Asian sources and ~ 35% for North American sources. The extent of these areas over North America and Asia decreased considerably above the second model level; above this level the areas were located mainly over heavily industrialized sections of the U.S. and China and mountainous regions of Central America (for example, Mexico City, a large source, is located at a height of 2240 m). Because the MRs of SO_2 from biogenic sources were considerably less than the H_2O_2 MRs, the time series of the fraction of SO_2 in areas where SO_2 was less than H_2O_2 for this source type showed little variability over time; however, the large day-to-day variability in volcanic emissions resulted in a large variability in the time series of this fraction for volcanic sources.

The domain-average fraction of SO_2 or sulfate in clouds was calculated as

$$\overline{F_{cl}} = \frac{\sum_{i,j} f_c A \sum_{k} f \, c_{sp} \Delta h_k}{\sum_{i,j} A \sum_{k} c_{sp} \Delta h_k}$$

where f_c is the cloud fraction for the grid cell (equal for all vertical levels), A is the area of the grid cell (m^2), f is equal to one if the LWVF was greater than 10^{-9} at vertical level k and equal to zero otherwise, c is the concentration (mol m^{-3}), sp denotes the species (SO_2 or sulfate), and Δh_k is the depth of model level k (m). Time series of the fraction of SO_2 in clouds by source region and source type, which reflected the daily cycle of clouds, exhibited very small variability for biogenic sources but large variability for volcanic sources. The amount of sulfate that encountered precipitating clouds was calculated by setting f equal to one if LWVF was greater than 10^{-9} at vertical level k and there was precipitation in the grid cell, and equal to zero otherwise. Time series of this quantity by source region and source type, which reflected the daily cycle of precipitation, showed fairly small variability, with the largest variability exhibited by sulfate from Asian sources.

Examination of the relative contributions of the SO_2 to sulfate oxidation pathways to the total sink of SO_2 and to the conversion of SO_2 to sulfate by source region and source type showed that the contribution of the aqueous-phase oxidation was the largest and the contribution of the gas-phase oxidation was the smallest for biogenic sources (Table 6). Almost all of the SO_2 from biogenic emissions (~ 94%) was located in regions where its MR was less than that of H_2O_2, so the large fraction of SO_2 converted via the fast aqueous-phase oxidation left a smaller fraction of the SO_2 to experience the slower gas-phase oxidation. In addition, the OH concentration in most of the areas of largest biogenic emissions (south of 20°N and north of 50°N, Figure 2) was generally smaller than over areas of largest anthropogenic and volcanic emissions. The contribution of the aqueous-phase oxidation to the total conversion of SO_2 to sulfate for biogenic SO_2 was the largest of all source types. The release heights of volcanic emissions were much higher than those for anthropogenic and biogenic emissions; thus the SO_2

from this source type was much less subject to dry deposition and the contribution of this sink to the total SO_2 sinks was the smallest of all source types. The smaller dry deposition rate allowed greater time for the conversion of SO_2 to sulfate by both conversion pathways; for this source type the contribution of the gas-phase oxidation to the total SO_2 sinks was the largest and the contribution of the aqueous-phase sink was the second largest; however, because of the large gas-phase conversion (a factor of 2 or more greater than for other source types) the contribution of the aqueous-phase oxidation to the total conversion of SO_2 to sulfate was the smallest of all sources.

The fraction of SO_2 in areas where the SO_2 MR was less than the H_2O_2 MR ranged from 56.1% for North American sources to 32.7% for Asian sources. The larger fraction for North American sources was the result of the HO_2 distribution, which showed larger concentrations over North America, especially over the eastern U.S. and Canada, coinciding with areas of largest emissions from these sources. The relative importance of the total aqueous-phase oxidation to the total sinks of SO_2 and to the conversion of SO_2 to sulfate is the result of a tradeoff between the relative amounts of SO_2 and H_2O_2 and the fraction of SO_2 in clouds. The greater fraction of SO_2 from North American sources in areas where the MR of SO_2 was less than the MR of H_2O_2 appears to have compensated for the smaller fraction of SO_2 in clouds, so the contribution of the aqueous-phase oxidation to the total SO_2 sinks was largest of all anthropogenic sources. The greater fraction of SO_2 in clouds for Asian sources appears to have compensated for the smaller fraction of SO_2 in areas where the MR of SO_2 was less than the MR of H_2O_2, so the contribution of the aqueous-phase oxidation to the total SO_2 sinks for these sources was the second largest. The fraction of SO_2 in clouds for European sources appears to have been unable to compensate for the smaller fraction of SO_2 in areas where the MR of SO_2

was less than the MR of H_2O_2, so the contribution of the aqueous-phase oxidation to the total SO_2 sinks for this source region was the lowest for all anthropogenic sources.

Turnover times for modeled SO_2 varied between 0.7 days for biogenic SO_2 and 2.2 days for volcanic SO_2 (Table 7). Biogenic SO_2 had the shortest turnover time because ~ 94% of this SO_2 was located in areas where the SO_2 MRs were less than the H_2O_2 MRs (Table 6), resulting in rapid conversion of SO_2 to sulfate. Volcanic SO_2 had the longest turnover time because the elevated release height of these emissions reduced their exposure to dry deposition. For anthropogenic emissions the relative length of the turnover time was a result of a tradeoff between the relative amounts of SO_2 and H_2O_2 and the fraction of SO_2 in clouds in an analogous way to the influence on the relative importance of the total aqueous-phase oxidation to the total sinks of SO_2 as discussed above.

Turnover times for modeled sulfate (Table 8) varied between ~ 4 days for sulfate from biogenic emissions to ~ 9 days for sulfate from volcano emissions; the overall turnover time for all sulfate was ~ 7 days. Wet deposition is the major sink for sulfate, so there appears to be an inverse relation between turnover time and the fraction of sulfate encountering precipitating clouds for each source region and source type. Volcanic (biogenic) sources have the longest (shortest) turnover time and the smallest (largest) fraction of sulfate encountering precipitating clouds. For anthropogenic emissions European sources have the longest turnover time and the smallest fraction of sulfate encountering precipitation clouds. These results may be compared to analyses of atmospheric measurements of natural and bomb-test radioactive species, which can be used as surrogates for accumulation mode aerosol particles, inferred turnover times of 5 to 10 days [*Chamberlain*, 1991]; analyses of measurements of the decay of atmospheric

concentrations of ^{137}Cs in the weeks following the Chernobyl accident inferred turnover times of 7 to 9 days [*Cambray et al.*, 1987].

The results presented here, which include analyses in three dimensions, may be contrasted with those of Koch et al. [2003], who found a significant negative correlation between observed daily cloud cover and surface sulfate concentrations in Europe and North America. However, the influence of other important factors in the aqueous-phase production of sulfate, such as cloud liquid water content and the relative concentrations of SO_2 and H_2O_2, were not included in their statistical analyses. Those investigators suggested that clouds inhibit sulfate (via inhibition of gas-phase production and scavenging by precipitation) more than they enhance it (via aqueous-phase production). Three experiments were conducted using the Goddard Institute for Space Studies General Circulation Model (GISS GCM) with online sulfur chemistry to consider the relative contributions of gas and aqueous-phase conversion pathways to the correlation behavior. The model did not identify the sulfate generated via aqueous-phase conversion that is rained out in the same event; if this sulfate were not included in the amount produced by this pathway the conclusion that models probably have excessive aqueous-phase generation of sulfate might need to be re-examined. A correction in the dissolved species scheme used in the model improved the correlation between clouds and surface sulfate, but resulted in a larger bias between modeled and observed surface sulfate.

The relative contribution of the several source types to the sulfate burden is somewhat different from their contribution to emissions (Table 4). Whereas volcanic sources represented ~ 6% of emissions, their contribution to the sulfate burden was ~ 10%; this is a consequence of the longer lifetime and higher sulfate yield. In contrast, biogenic sources contributed ~13% of the emissions, but only ~ 5% of the burden; this is a consequence of the shorter lifetime of

sulfate from these sources. Anthropogenic sources contributed slightly less to the emissions (~ 80%) than to the sulfate burden (~ 84%). The fractional contribution of North American and Asian sources to emissions and to the sulfate burden was within ~ 1%; however, due to the larger yield and longer residence time of sulfate (Table 8) from European sources, these sources contributed ~ 5% more to the burden than to the emissions. The contribution of the several source types to the SO_2 burdens is similar to the contribution to the sulfate burden except that because of the different turnover times anthropogenic sources contribute somewhat less and volcanic sources contribute somewhat more. Volcanic emissions have the largest sulfate potential, defined [*Rasch et al.*, 2000a] as the ratio of the sulfate burden to the SO_2 emissions, by a factor of between 1.4 and 2.4 (Table 8), and biogenic emissions have the smallest; emissions from European sources have the largest ratio of all the anthropogenic emissions, and emissions from North America have the smallest. These results are driven by differences in turnover times and the importance of conversion pathways and removal mechanisms of the different source types as discussed above.

Based on the results of the present study (which includes the period June-July 1997 only) the mean burden in the model domain (Table 4) was estimated at 0.59 Tg S for sulfate and 0.20 Tg S for SO_2. These values must be expected to be larger for sulfate and smaller for SO_2 than those from simulations for a full year because both species exhibit a seasonal cycle (more conversion and therefore more sulfate and less SO_2 in the summer; less conversion and therefore less sulfate and more SO_2 in the winter), and are somewhat less than global values because of the limited geographic domain of the model. Feichter et al. [1997] estimated that 69% of the sulfate and 76% of the SO_2 are found in the Northern Hemisphere.

In contrast to the study presented here, which consisted of an 8-week simulation of the Northern Hemisphere for June-July 1997 at 1°×1° and 27 vertical levels using meteorological information specific to those times and locations and additional model input data adjusted as much as possible to reflect the simulation period, previous modeling studies have for the most part performed global and generally multi-year simulations at coarser resolutions, some incorporated into a GCM or using output from a GCM. Two studies that presented information on the influences of source regions and/or source types on sulfate burdens are compared with results presented here. These studies both used meteorological information generated by a GCM and presented averages over several simulation years. Graf et al. [1997] examined the source strength of volcanic SO_2 emissions and their contribution to the global sulfate distribution using a coupled climate-chemistry GCM with 3.75° resolution in the vertical and 19 vertical levels to 10 hPa. No primary anthropogenic sulfate emissions were included, and DMS was converted to SO_2 only. A 3-month spin up time was allowed, and global averages from a 5-yr simulation were presented. Volcanic emissions had the largest sulfate potential (called efficiency by Graf et al.) and anthropogenic emissions the smallest, and the contribution of volcanic emissions to the sulfate burden was almost as much as the contribution from anthropogenic emissions, a much greater fraction from that found in the study presented here. Although lack of detailed information in the Graf paper precludes a full explanation of all the reasons that could account for the differences with the study presented here, several factors can be listed. In the Graf et al. study total Northern Hemisphere emissions were larger (79 Tg S yr^{-1}), the relative contributions of the various source types was different (biogenic ~ 9.5%, anthropogenic ~ 78%, volcanic ~ 13%) compared to values from the present study (Table 4), and the distribution of the volcanic emissions was fairly different (for example, volcanos in Iceland and the Kamchatka

Peninsula had greater emissions). A large fraction of anthropogenic sources and some of the larger emitting volcanos were located in midlatitudes, where there is a strong seasonal signal in oxidant concentrations and reaction rates; in contrast, a large fraction of the biogenic sulfate is generated south of 30°N, where the seasonal signal is not as pronounced, altering the relative conversion of these emission sources depending on the season and impacting the annual values presented in their study.

Rasch et al. [2000a] performed a study using the National Center for Atmospheric Research's GCM (Community Climate Model Version 3, CCM3) with 2.8° horizontal resolution and 18 vertical levels to 35 km. The sulfur cycle was included in the GCM, and oxidant concentrations were prescribed from fields generated in an independent run of the Intermediate Model of Global Evolution of Species (IMAGES) [*Müller and Brasseur*, 1995]. A three year simulation was performed with the sulfur components tagged by region of origin. In this simulation CCM3 had several biases that directly impacted the sulfur cycle: the amplitude of the seasonal cycle of precipitation over the continental US was larger than observations, maxima in spring and minima in late fall in precipitation over Central Europe not seen in observations, and low summertime cloud cover over continents. The two most important processes controlling sulfate were identified as the aqueous-phase conversion of SO_2 and the wet deposition sink of sulfate, both of which are highly dependent on the meteorological information on clouds and precipitation. Annual average global sulfate and SO_2 burdens were 0.60 Tg S and 0.4 Tg S respectively. Regions denoted North America and Europe were defined in limited latitude ranges (15°-90°N for North America, 21°-90°N for Europe), and biogenic emissions were divided according to these geographic regions; thus direct comparisons with results from the present study are difficult. The emissions inventories used by Rasch et al. reflected emissions

ca. 1985, which included larger emissions in North America and Europe and smaller emissions in Asia than the inventory used in the study presented here, which reflected emissions ca. 1995. For North American and Asian emissions the anthropogenic sulfate potential was similar in Rasch et al. and in the study presented here (Table 8); however, the sulfate potential for European emissions is significantly lower in Rasch et al. (attention is called to error in Figure 5 of Rasch et al.; the units should be Gg not Tg). There could be several reasons for this difference. European emissions were large and were located mainly north of 40°N, where the oxidant cycle has a large seasonal signal, influencing yearly averages when compared to values for a specific summer season. In addition, the strong northwest flow over Europe in June-July 1997 transported European emissions south of 21°N (an area not included in the Rasch et al. definition of the European region) where large OH concentration, sparse precipitation, and high temperatures promoted additional gas-phase oxidation of SO_2 and slower removal of sulfate.

Several studies (briefly summarized in Table 9) were selected for comparison of key physical diagnostic quantities. In addition to the differences indicated in the table key processes differed in many respects among these studies, including emissions inventories, parameterizations of transport, chemical mechanisms, and wet and dry deposition. The summer simulation for June-July 1986 in Benkovitz and Schwartz [1997] using Version 1 of the present model is also included. The rates of the several removal processes of sulfate and SO_2 for the models (Table 10) show marked model-to-model differences for key processes. For example the rates of dry deposition and aqueous-phase oxidation of SO_2 range over a factor of three. The present model exhibits the highest aqueous-phase conversion rate of the several models (51% day^{-1}); this removal process includes aqueous-phase reaction which forms sulfate that remains in the atmosphere (30% day^{-1}) and that is removed in the time step in which it is formed

(reactive rainout, 21% day^{-1}); it is not clear to what extent the rate of aqueous conversion in the other models is lower because it encompasses only sulfate which remains in the atmosphere. The high aqueous-phase removal rate in the present model results in a lifetime of SO_2 (1.1 days) which is considerably shorter than values determined in previous studies (1.8 to 2.8 days, the latter value from a study using Version 1 of the present model). Certainly some of the model-to-model differences may be reflective of the different meteorological conditions and geographical domains treated in the models; this conclusion gains support in the fact that the lifetimes of SO_2 from the several source types examined in the present model vary from 0.7 day (biogenic, Table 7) to 2.2 days (volcanic). Nonetheless it would seem evident that substantial differences in removal rates in the several models are due to differences in treatment of the pertinent processes. Despite considerable differences in removal rates, the fraction of SO_2 that is removed by the several processes may be rather similar (e.g., the present model and that of Lelieveld et al. [1997]). Likewise despite the aqueous conversion in the present model being approximately twice as fast as in the model of Roelofs et al. [1998], that model indicates the fraction of SO_2 that is removed by aqueous conversion to be even greater than in the present model. Also presented in Table 10 is a comparison of the sulfate potential for several models, calculated as sulfate burden divided by the SO_2 emissions, which differs by more than a factor of almost a factor of two. Considerations such as these underscore the need to examine key physical diagnostics in model comparisons, rather than simply assessing how well the models reproduce observed mixing ratios, as well as the potential utility of comparing such diagnostics with measurements from field studies. For detailed studies of the influence of aerosols on climate model representations, input data, evaluations with observations, and key physical

diagnostics need to be examined in detail to try to elucidate the reasons for model-to-model differences and reduce them.

In addition to the turnover times the main difference between Benkovitz et al. [1994] and the present study, the relative importance of the SO_2 sinks, can be explained by several factors. The meteorological conditions were different for the time periods of the two simulations. The meteorological data for the June-July 1986 study did not include cloud LWC information; the cloud model used calculated the LWC only for precipitating clouds, limiting the extent of the aqueous phase oxidation of SO_2. A limiting reagent formulation for the aqueous phase conversion by H_2O_2 was used in June-July 1986 study; this approach overestimates the oxidation of SO_2. In order to compare the relative conversion via the limiting reagent and via the full chemistry formulations a 1-h simulation was performed using the limiting reagent formulation in Version 2 of GChM-O. In 94% of the locations where SO_2 was oxidized by H_2O_2, SO_2 was the limiting reagent; this fraction would be expected to vary for different seasons. The full kinetics mechanism always generated less sulfate; for the whole domain this mechanism generated only 44% of the sulfate generated by the limiting reagent mechanism.

In the work presented here a large fraction of the discrepancies between the modeled and observed sulfate and SO_2 mixing ratios seems to be explained by the subgrid variability and measurement errors of these quantities. However, while overall the modeled sulfate concentration in precipitation was within a factor of 3 of the observed concentration, almost 75% of the concentrations were overestimated by the model, ~ 17% with $S_{m/o}$ values greater than 8. Values for the sulfate turnover times were close to those obtained from measurements of accumulation mode particles associated with the release of radionuclides. The relative values of

key diagnostic quantities (turnover times, oxidation rates, etc.) by source region and source types can be understood in terms of the meteorological conditions prevalent during the simulation.

A question that always needs to be asked in any modeling exercise is: are we getting the "right answers" for the "wrong reasons"? A possible reason for the closer agreement between modeled and observed sulfate and SO_2 MRs than for sulfate concentration in precipitation is that the SO_2 emissions and the oxidant concentrations were overestimated and the excess sulfate generated was removed by wet deposition, either because of deficiencies in the algorithms used for wet removal and the incorporation of aerosols into cloud water or because of overestimation of the precipitation values used by the model. Therefore, several points of concern need to be addressed in the continued development and use of GChM-O. The wet removal algorithm used was a simplified representation which needs further testing and refinement. In addition it does not account for either evaporation of falling precipitation in non-cloudy layers or below-cloud scavenging of aerosols; the importance of these processes needs to be examined, and if results indicate they are significant these processes must be represented in the algorithm. The algorithm used to represent the incorporation of aerosols into cloud water also needs further development and testing; for example, the values selected for f_{max}, L_{mid}, and the limiting cloud liquid water fraction need to be further evaluated, although the overall rate of this process is likely much more sensitive to the frequency of encountering clouds than to the value of these parameters.

The values of the oxidant MRs used were averages from a model that used meteorology from a GCM. As the GCM values did not reflect the actual meteorological conditions at the times and locations of the simulation, model simulations might be improved by use of more accurate representation of the oxidant MRs, which can be obtained if these MRs are calculated online in the CTM. Emissions for some regions and source types can vary significantly from

year to year, especially for highly time-dependent sources such as volcanos and biogenic sources; more accurate emissions for the simulation period are needed, including more detailed breakdowns by season, release height, percent released as primary sulfate, and quantitative values of the uncertainties of these emissions.

A two-week model spinup time was used for the simulation presented here; time series plots of certain quantities such as sulfate yield indicated that a longer spinup time would have been more appropriate for a simulation over the Northern Hemisphere domain used. Future simulations using this domain would seem to require a spinup time of approximately one month.

6. Summary and Conclusions

An Eulerian chemical transport model (CTM) for sulfate, the Global Chemistry Model driven by Observation-derived meteorology (GChM-O), has been developed to represent the sulfur cycle and to calculate distributions of sulfate, SO_2, DMS, and MSA with high spatial and temporal resolution, for specific times and locations, identified by source region, source type, and formation process. The model has been used to simulate the ACE-2 experimental period (June-July 1997) over the Northern Hemisphere from the equator to 81°N at 1°×1° resolution and 27 vertical levels.

Modeled MRs of sulfate and SO_2 and concentrations of sulfate in precipitation were evaluated using daily averaged sulfate and SO_2 MRs and event or weekly sulfate concentration in precipitation from observations by monitoring stations in North America, Europe, Taiwan, and stations in the Canary Islands and Korea. Concerns arise in these evaluations from lack of representativeness of the observational data sets. Many of the stations were under meteorological continental influence and were at least periodically impacted by proximate sources. In addition, for the majority of evaluations observed MRs for a model grid cell were

based on a single monitoring station; thus cell-averaged model results were evaluated using point observations within the corresponding cell. This effect was examined and quantified using the median ratio characteristic spread (a measure of the variation of the ratios of observed quantities) of simultaneous observations which provided the spatial variability within model grid cells and qualified the level of agreement that might be expected between modeled and observed quantities, especially for primary emitted species such as SO_2 or for sporadic phenomena such as precipitation. Median ratio characteristic spreads for simultaneous observations were 1.33 for sulfate, 2.32 for SO_2, and 1.36 for sulfate concentration in precipitation.

The characteristic spreads between modeled and observed MRs for sulfate (5083 cases, median 1.85) and SO_2 (24155 cases, median 2.55) were comparable to, although somewhat greater than, those between observed MRs, indicating that departure between modeled and observed MRs was due in large part to the subgrid variation of the observed MRs. The median value of the characteristic spread between modeled and observed sulfate concentration in precipitation (2044 cases, median 2.82) was considerably larger than the spread between observations (127 cases, median 1.36), influenced in part by the proximate locations of stations within a grid cell and by differences between the precipitation used in the model and the actual precipitation at the monitoring stations.

The differences between the modeled and observed MRs (a measure of model bias) for sulfate and SO_2 peaked at low values; the peaks included substantial contributions from a wide range of values of the observed MRs. The model almost equally overestimated and underestimated the sulfate observed MRs and overestimated somewhat over half of the SO_2 observed MRs. Over half of the modeled sulfate MRs were within a factor of 2 of the observed MRs, and over half of the modeled SO_2 MRs were within a factor of 3 of the observed MRs.

Time series of the sulfate MRs demonstrated that model results closely track the magnitudes and temporal episodicity of the observed MRs.

The major sink for sulfate and MSA was wet deposition (84 to 92% for sulfate, 87% for MSA); the two major sinks for SO_2 were aqueous-phase conversion to sulfate (50 to 69%) and dry deposition (6 to 29%), except for emissions from volcanic sources for which gas-phase conversion exceeded dry deposition. For sulfate and SO_2 turnover times differed substantially depending on source type, for sulfate from 4.3 to 9.0 days and for SO_2 from 0.7 to 2.2 days; turnover times were 3.9 days for MSA, and 1 day for DMS. Aerosol sulfate yields also differed substantially depending on source type, from 45 to 64%, and the MSA yield was 11%.

Comparison of the results of this study with results from two previous studies that included analyses by source type or source region found discrepancies in the relative importance of sources on the resulting sulfate burden; in addition to differences in process representations in the models these discrepancies are influenced by the different meteorological conditions, emissions estimates, and length of the simulations presented (annual averages vs. a specific summer). Discrepancies of a factor of 2 or more remain in the removal rates, burden, lifetime, and contribution to sinks of both sulfate and SO_2 determined by the present study and those of other investigators. These differences directly affect the determination of the influence of aerosols on climate, indicating a need to examine the model representations, input data, and to evaluate with observations to try to elucidate and reduce these differences.

In conclusion, the three-dimensional chemical transport model for sulfur described here is a powerful tool for examining sulfur mixing ratios and burdens by source region, source type, and formation process on a hemispheric to global scale, pertinent to the issues of radiative forcing by sulfate aerosol. Evaluation of sulfate and SO_2 MRs demonstrates that the model

represents the observed sulfate and SO_2 MRs at fine temporal resolution with an accuracy comparable to the spatial variability and measurement error of the observed MRs. These analyses also demonstrate the importance of driving the model with meteorological quantities and other model input data representing as accurately as possible the conditions at the time when the observations were made.

Appendix A

Calculation of Mixed Layer Heights

Time- and location-dependent mixed layer heights were obtained by a multi-step approach based on calculated values of the equivalent potential temperature (θ_e), the saturation equivalent potential temperature, (θ_{es}), the dew point, (T_d), and the height (above ground) of the model vertical levels. For every model grid cell (1° × 1°), referred to as a location, each successive step was applied only if the conditions of the previous steps were not met.

1) Convective cloud cases were identified when the meteorological data showed convective precipitation and a cloud base height less than 2 km. For these conditions air parcels rise through the mixed layer and then continue rising until they reach neutral buoyancy near the cloud top. A separate convective mixing algorithm was used within the cloud layer; therefore the mixing depth was set to the height of cloud base. 2) If no precipitation occurred the grid cell the thermodynamic profile was tested for convective instability. Profiles were defined as convectively unstable when θ_e at the surface exceeded θ_{es} at any height [*Bohren and Albrecht*, 1998]. A simplified parcel theory was used to approximate the depth of the mixing layer as the lowest level at which a parcel rising from the surface achieved neutral buoyancy (also called the level of free convection, LFC) under the assumption of a constant entrainment rate of 30% km^{-1} [*Gregory*, 2001]. When the LFC exceeded 4 km, the entrainment rate was decreased in steps of

1% km^{-1} until the height of the LFC was less than 4 km. 3) If no LFC below 4 km was found, convective boundary layer profiles were identified by testing for the presence of a subsidence inversion manifest in the decrease of humidity across the inversion. The mixing layer depth was defined as the height, less than or equal to X km, where the decrease in T_d between two successive model levels was 4K or less; X was taken as 4 km for latitudes 0 to 15°N, as 3 km for latitudes 15°N to 60°N [*Albrecht et al.*, 1995] and as 2 km for latitudes greater than 60°N [*Uttal et al.*, 2002]. 4) For locations that did not satisfy any of these criteria the vertical profile was considered to be stable (i.e. parcels displaced vertically tend to return to their original level), and the mixed layer height was set to the height of the first model level above the surface.

Appendix B

Calculation of DMS Emissions from the Ocean

Time- and location-dependent dimethylsulfide (DMS) emissions from the ocean were estimated using sea surface DMS concentrations and the wind speed transfer function of Liss and Merlivat [1986]. The data source for the sea surface DMS concentrations was the global data set compiled by Kettle et al. [*Kettle et al.*, 1999], which includes over 15,000 point measurements throughout the world oceans taken between March 1972 and October 1997. DMS concentrations in mid and high latitudes have a strong seasonal dependency [*Kettle et al.*, 1999]; the timing of this seasonality depends on a combination of physical, chemical and biological processes. The DMS measurements in the Kettle et al. database for June and July were used for the Atlantic and Pacific Oceans; the selected data included only open-ocean measurements as coastal and estuarine DMS concentrations are generally higher than open ocean concentrations and representative of only small areas around the measurement location. A water depth of 100

m was used to differentiate between open-ocean and coastal measurements (C. Wirick, Brookhaven National Laboratory, personal communication, 1999). The selected data set included 646 measurements in the Atlantic Ocean and 191 measurements in the Pacific Ocean.

The surface DMS concentrations chosen were used to create a 1°×1° resolution grid using a geostatistical methodology known as kriging [*Isaaks and Srivastava*, 1989]. Kriging generates an estimated surface from a scattered set of points based on regionalized variable theory that assumes that the same pattern of variation can be observed at all locations on the surface. Kriging is an excellent linear unbiased estimator because 1) low weights are assigned to distant samples and higher weights to proximate samples, and 2) the relative position of the samples to each other as well as the area being examined are taken into account. The spatial variation is quantified by a semi-variogram; the semi-variogram is modeled by fitting a theoretical function to the sample semi-variogram. The Geographic Information System software Arc/Info used assumes that the variation in the values is free from any structural component. The surface estimator can be calculated using spherical, circular, exponential, gaussian and linear methods. Kriging uses the mathematical function selected to fit a line or curve to the semi-variance data in the semi-variogram. For each ocean, the DMS concentrations were krigged using each of the five methods indicated above for several cell resolutions. The optimum cell size and method were selected to maintain the regional features in the DMS data set but to eliminate small hot-spots.

Within the ACE-2 study area the ACE-2 surface DMS data were used, as these measurements best reflected the conditions for June-July 1997 [*Bates et al.*, 2000]. Measurements showed that the sea surface temperature and salinity in the experimental region varied linearly with latitude ranging from 23°C, 36.8 PSU in the south (29°N) to 18°C, 35.8 PSU

in the north (41°N). Surface seawater DMS concentrations during ACE-2 were relatively uniform during the first 3 weeks of the campaign averaging 1.3 ± 0.2 nM for distances greater than 40 km from the Portugal coast, which is outside the upwelling waters identified on the basis of temperature and salinity. During the final week, concentrations in the offshore region west of Portugal began to increase, reaching 2.7 nM by the end of the campaign [*Bates et al.*, 2000]. The field measurements were krigged over the experimental area and used to replaced the Kettle et al. krigged values.

Sea-surface temperatures from the Kettle et al. data base were gridded using the same procedure. The gridded temperature and DMS sea surface concentrations were combined with ECMWF wind speeds at 6-hr intervals to calculate DMS emission fluxes using the Liss and Merlivat wind-speed transfer velocity relationship

Appendix C

Summary of Observations Used in Model Evaluation

The sulfate observational data set consisted of 6067 measurements at 481 stations in 12 different networks; sampling duration times varied from 1 to 7 days, with over 90% of the sampling being 1 day or less. Almost 50% of the measurements were from the EMEP network (Figure C-1a), ~ 23% were from the AIRS network, with the rest of the networks each contributing 10% or less. After averaging concurrent measurements at each location to obtain the observed MRs there were 5083 cases available at 320 locations. The majority of the observed MRs (~ 63%) were less than or equal to 0.66 ppb, with ~ 3% greater than 3 ppb. There were concurrent measurements in ~ 6% of the cases; all cases were located in North America except for those at the ACE-2 stations at Tenerife, Canary Islands. The multiple observations set

exhibited somewhat greater MRs than the data set as a whole (Figure C-2a), probably a reflection of greater density of measurements in locations with larger sulfate MRs in support of air quality assessment or compliance.

The SO_2 observational data set included 24155 measurements from 893 stations in 10 different networks; sampling duration times (or reported averaging times in the case of real-time instruments) varied from 1-h to 7 days, with over 98% of the sampling being 24-h or less. The measurements were averaged to 24-h when needed; little is gained in evaluating 6-h modeled MRs with 6-h averaged observed MRs as versus the 24-h averages [*Benkovitz and Schwartz*, 1997]. Almost 70% of the measurements were from the AIRS network (Figure C-1b), with the rest of the networks each contributing ~ 10% or less. After averaging concurrent measurements in each location to obtain the observed MRs there were 12624 cases available at 414 locations. The majority of the observed MRs (~ 55%) were less than or equal to 3 ppb, with ~ 7% greater than 10 ppb. There were concurrent measurements in ~ 28% of the cases; all are located in North America except for some cases located in Taiwan. For the multiple observations set (Figure C-2b) very few MRs were less than 1 ppb, with the majority (~ 63%) in the 3 to 10 ppb range; in contrast for the entire data set almost 25% of the MRs were less than 1 ppb, with the majority (~ 54%) less than or equal to 3 ppb.

There were a total of 521 evaluation locations for sulfate or SO_2; ~ 20% had sulfate observations only, ~ 39% had SO_2 observations only and ~ 41% had both sulfate and SO_2 observations.

The concentration of sulfate in precipitation was measured by 11 networks with 369 stations; observed concentrations corrected for sea salt sulfate were used in these evaluations. The networks monitored 2366 events, of which 2187 (~ 92%) were captured in the

model (ie, the meteorological data indicated rain within the time period for which precipitation was collected), from 100% for more than half of the networks to 84% for EMEP. The EMEP network contributed the highest number of events, (Figure C-1c), followed by NADP and CAPMoN, with the rest of the networks contributing substantially less. After averaging concurrent measurements in each location to obtain the observed concentrations there were 2044 cases available for evaluation at 316 locations. The majority of the observed concentrations (~ 51%) were less than or equal to 15 μmol L^{-1}, with ~ 13% greater than 40 μmol L^{-1}. There were concurrent measurements in ~ 6% of the cases.

Acknowledgments. Research by BNL investigators was performed under the auspices of the U.S. Department of Energy under Contract No. DE-AC02-98CH10886. The meteorological data used to drive the model were obtained from the European Centre for Medium-Range Weather Forecasts (ECMWF), Reading, UK. As listed in Table 5, some of the sulfate and wet deposition data used in this work were provided by the Canadian National Atmospheric Chemistry (NatChem) Database and its data contributing agencies and organizations. We thank the principal investigators listed in Table 3 for supplying the measurements of volcanic SO_2 emissions. We thank M. Altaf Mubaraki for his help in this project.

References

Albrecht, B.A., M.P. Jensen, and W.J. Syrett, Marine Boundary Layer Structure and Fractional Cloudiness, *J. Geophys. Res.. 100* (D7), 14209-14222, 1995.

Andres, R.J., and S.D. Kasgnoc, A Time-Averaged Inventory of Subaerial Volcanic Sulfur Emissions, *J. Geophys. Res.*, *103*, 25251-25261, 1998.

Barrie, L.A., Y. Yi, W.R. Leaitch, U. Lohmann, P. Kasibhatla, G.-J. Roelofs, J. Wilson, F. McGovern, C. Benkovitz, M.A. Mélières, K. Law, J. Prospero, M. Kritz, D.Bergmann, C. Bridgeman, M. Chin, J. Christensen, R. Easter, J. Feichter, C. Land, A. Jeuken, E. Kjellström, D. Koch, and P. Rasch, A Comparison of Large Scale Atmospheric Sulphate Aerosol Models (COSAM): Overview and Highlights, *Tellus*, *53B*, 615-645, 2001.

Barth, M.C., P.J. Rasch, J.T. Kiehl, C.M. Benkovitz, and S.E. Schwartz, Sulfur Chemistry in the National Center for Atmospheric Research Community Climate Model: Description, Evaluation, Features and Sensitivity to Aqueous Chemistry, *J. Geophys. Res.*, *105* (D1), 1387-1415, 2000.

Bates, T.S., B.K. Lamb, A. Guenther, J. Dignon, and R.E. Stoiber, Sulfur Emissions to the Atmosphere from Natural Sources, *J. Atmos. Chem.*, *14*, 315-337, 1992.

Bates, T.S., P.K. Quinn, D.S. Covert, D.J. Coffman, J.E. Johnson, and A. Wiedensohler, Aerosol Physical Properties and Processes in the Lower Marine Boundary Layer: A Comparison of Shipboard Sub-Micron Data from ACE-1 and ACE-2, *Tellus*, *52B*, 258-272, 2000.

Benkovitz, C.M., H. Akimoto, J.J. Corbett, J.D. Mobley, J.G.J. Olivier, J.A.v. Aardenne, and V. Vestreng, Compilation of Regional to Global Inventories of Anthropogenic Emissions, in *Emissions of Atmospheric Trace Compounds*, edited by C. Granier, P. Artaxo, and C.E. Reeves, pp. 19-78, Kluwer Academic Publishers, Dordrecht, The Netherlands, 2004.

Benkovitz, C.M., J.J.M. Berdowski, M.A. Mubaraki, and J.G.J. Olivier, Global Anthropogenic Sulfur Emissions for 1985 and 1990, in *Assessing Historical Global Sulfur Emission Patterns for the Period 1850-1990*, edited by A.S. Lefohn, J.D. Husar, and R.B. Husar, pp. A1-A45, U.S. Department of Energy, Washington, DC, 1996.

Benkovitz, C.M., C.M. Berkowitz, R.C. Easter, S. Nemesure, R. Wagener, and S.E. Schwartz, Sulfate Over the North Atlantic and Adjacent Continental Regions: Evaluation for October and November, 1986 Using a Three-Dimensional Model Driven by Observation-Derived Meteorology, *J. Geophys. Res.*, *99* (D10), 20725-20756, 1994.

Benkovitz, C.M., and S.E. Schwartz, Evaluation of Modeled Sulfate and SO_2 over North America and Europe for Four Seasonal Months in 1986-87, *J. Geophys. Res.. 102* (D21), 25305-25338, 1997.

Benkovitz, C.M., S.E. Schwartz, and B.-G. Kim, Evaluation of a Chemical Transport Model for Sulfate using ACE-2 Observations and Attribution of Sulfate Mixing Ratios to Source Regions and Formation Processes, *Geophys. Res. Let.*, *30* (12), 10.1029/2003GL016942, 2003.

Bohren, C.F., and B.A. Albrecht, *Atmospheric Thermodynamics*, 402 pp., Oxford University Press, New York, NY, 1998.

Brasseur, G., D. Hauglustaine, S. Walters, P. Rasch, J. Müller, G. Granier, and X.X. Tie, MOZART: A Global Chemical Transport Model for Ozone and Related Chemical Tracers. 1. Model Description, *J. Geophys. Res.*, *103* (D21), 28265-28289, 1998.

Brasseur, G.P., and S. Madronich, Chemistry-Transport Models, in *Climate System Modeling*, edited by K.E. Trenberth, pp. 491-518, Cambridge University Press, New York, NY, 1992.

Cambray, R.S., P.A. Cawse, J.A. Garland, J.A.B. Gibson, P. Johnson, G.N.J. Lewis, D. Newton, L. Salmon, and B.O. Wade, Observations on Radioactivity from the Chernobyl Accident, *Nucl. Energy*, *26*, 77-101, 1987.

Chamberlain, A.C., *Radioactive Aerosols*, Cambridge University Press, New York, NY, 1991.

Charlson, R., S.E. Schwartz, J.M. Hales, R.D. Cess, J. J.A. Coakley, J.E. Hansen, and D.J. Hoffman, Climate Forcing by Anthropogenic Aerosols, *Science*, *255*, 423-430, 1992.

Cherubini, T., A. Ghelli, and F. Lalaurette, Verification of Precipitation Forecasts over the Alpine Region Using a High Density Observing Network, in *ECMWF Technical Memorandum*, pp. 18, European Centre for Medium-Range Weather Forecasts, Reading, UK, 2001.

Chin, M., R.B. Rood, S.-J. Lin, J.-F. Müller, and A.M. Thompson, Atmospheric Sulfur Cycle Simulated in the Global Model GOCART: Model Description and Global Properties, *J. Geophys. Res.*, *105* (D20), 24671-24687, 2000a.

Chin, M., D.L. Savoie, B.J. Huebert, A.R. Bandy, D.C. Thornton, T.S. Bates, P.K. Quinn, E.S. Saltzman, and W.J.D. Bruyn, Atmospheric Sulfur Cycle Simulated in the Global Model GOCART: Comparison with Field Observations and Regional Budgets, *J. Geophys. Res.*, *105* (D20), 24689-24712, 2000b.

Cowling, E.B., Acid Precipitation in Historical Perspective, *Environ. Sci. and Technol.*, *16*, 110A-123A, 1982.

Daum, P.H., S.E. Schwartz, and L. Newman, Acidic and Related Constituents in Liquid Water Stratiform Clouds, *J. Geophys. Res.*, *89*, 1447-1458, 1984.

Easter, R.C., and D.J. Luecken, A Simulation of Sulfur Wet Deposition and Its Dependence on the Inflow of Sulfur Species to Storms, *Atmos. Environ.*, *22* (12), 2715-2739, 1988.

Elias, T., A.J. Sutton, J.B. Stokes, and T.J. Casadevalt, Sulfur Dioxide Emission Rates of Kilauea Volcano, Hawaii, 1979-1997, pp. 41, Hawaiian Volcano Observatory, U.S. Geological Survey, Hawaii National Park, 1998.

Erickson, R.E., L.M. Yates, R.L. Clark, and D. MacEwen, The Reaction of Sulfur Dioxide with Ozone in Water and its Possible Atmospheric Significance, *Atmos. Environ.*, *11*, 813-817, 1977.

European Centre for Medium-Range Weather Forecasts, IFS Documentation Cycle CY25r1 Parts I - VII, European Centre for Medium-Range Weather Forecasts, Reading, England, 2003.

Feichter, J., U. Lohmann, and I. Schult, The Atmospheric Sulfur Cycle in ECHAM-4 and Its Impact on the Shortwave Radiation, *Climate Dynamics*, *13*, 235-246, 1997.

Goldberg, R.N., and V.B. Parker, Thermodynamics of Solution of SO_2 (g) in Water and of Aqueous Sulfur Dioxide Solutions, *J. Res. Natl. Bureau of Standards*, *90* (5), 341-358, 1985.

Graf, H.-F., J. Feichter, and B. Langmann, Volcanic Sulfur Emissions: Estimates of Source Strenght and Its Contribution to the Global Sulfate Distribution, *J. Geophys. Res.*, *102* (D9), 10727-10738, 1997.

Gregory, D., Estimation of entrainment rate in simple models of convective clouds, *Quart. J. Roy. Meteor. Soc.*, *127*, 53-72, 2001.

Guenther, A., C.N. Hewitt, D. Erickson, R. Fall, C. Geron, T. Graedel, P. Harley, L. Klinger, M. Lerdau, W.A. McKay, T. Pierce, B. Scholes, R. Steinbrecher, R. Tallamraju, J. Taylor, and P. Zimmerman, A Global Model of Natural Volatile Organic Compound Emissions, *J. Geophys. Res.*, *100* (D5), 8873-8892, 1995.

Haywood, J.M., and K.P. Shine, The effect of anthropogenic sulfate and soot aerosol on the clear sky planetary radiation budget, *Geophys. Res. Lett.*, *22*, 603-606, 1995.

Heald, C.L., D.J. Jacob, P.I. Palmer, M.J. Evans, G.W. Sachse, H.B. Singh, and D.R. Blake, Biomass burning emission inventory with daily resolution: Application to aircraft observations of Asian outflow, *J. Geophys. Res.. 108* (D21), doi:8811, 2003.

Hoigné, J., H. Bader, W.R. Haag, and J. Staehelin, Rate Constants of Reactions of Ozone with Organic and Inorganic Compounds in Water - III, *Water Res.*, *19* (8), 993-1004, 1985.

Horowitz, L.W., S. Walters, D. Mauzerall, L. Emmons, P. Rasch, C. Granier, X. Tie, J.F. Lamarque, M. Schultz, and G. Brasseur, A global simulation of tropospheric ozone and related tracers: Description and evaluation of MOZART, version 2, *J. Geophys. Res.*, *108* (D24), 4784, doi:10.1029/2002JD002853, 2003.

Isaaks, E.H., and R.M. Srivastava, *An Introduction to Applied Geostatistics*, Oxford University Press, New York, NY, 1989.

Jaffe, D., I. McKendry, T. Anderson, and H. Price, Six 'New' Episodes of Trans-Pacific Transport of Air Pollutants, *Atmos. Environ.*, *37*, 391-404, 2003.

Jung, T., and A. Tompkins, Systematic Errors in the ECMWF Forecasting System, in *ECMWF Technical Memorandum*, pp. 72, European Centre for Medium-Range Weather Forecasts, Reading, UK, 2003.

Kettle, A.J., and M.O. Andreae, Flux of dimethylsulfide from the Oceans: A Comparison of Updated Data and Flux Models, *J. Geophys. Res.*, *105* (D22), 26793-26808, 2000.

Kettle, A.J., M.O. Andreae, D. Amoroux, T.W. Andreae, T.S. Bates, H. Berresheim, H. Bingemer, R. Boniforti, M.A.J. Curran, G.R. DiTullio, G. Helas, G.B. Jones, M.D. Keller, R.P. Kiene, C. Leck, M. Levasseur, G. Malin, M. Maspero, P. Matrai, A.R. McTaggart, N. Mihalopoulos, B.C. Nguyen, A. Nuovo, J.P. Putaud, S. Rapsomanikis, G. Roberts, G. Schbeske, S. Sharma, R. Simo, R. Staubes, S. Turner, and G. Uher, A Global DataBase of Sea Surface Dimethyl Sulfide (DMS) Measurements and a Procedure to Predict Sea Surface DMS as a Function of Latitude, Longitude, and Month, *Global Biogeochm. Cycles*, *13*, 399-444, 1999.

Ko, M.K., and N.-D. Sze, Impact on Stratospheric Ozone from Emissions of CFCs and Substitutes: a Two-Dimensional Model Assessment, in *Atmospheric Chemistry Models and Predictions for Climate and Air Quality*, edited by C.S. Sloane, and T.W. Tesche, pp. 9-24, Lewis Publishers, Inc., Chelsea, MI, 1991.

Koch, D., D. Jacob, I. Tegen, D. Rind, and M. Chin, Tropospheric Sulfur Simulation and Sulfate Direct Radiative Forcing in the Goddard Institute for Space Studies General Circulation Model, *J. Geophys. Res.*, *104* (D19), 23799-23822, 1999.

Koch, D., J. Park, and A.D. Genio, Clouds and Sulfate are Anticorrelated: A New Diagnostic for Global Sulfur Models, *J. Geophys. Res.. 108* (D24), doi:10.1029/2003JD003621, 2003.

Kuylenstierna, J.C.I., H. Rodhe, S. Cinderby, and K. K. Hicks, Acidification in developing countries; Ecosystem sensitivity and the critical load approach on a global scale, *Ambio*, *30*, 20 - 28, 2001.

Lalaurette, F., L. Ferranti, A. Ghelli, and G.v.d. Grijn, Verification Statistics and Evaluations of ECMWF Forecasts in 2002-2003, in *ECMWF Technical Memorandum*, pp. 48, European Centre for Medium-Range Weather Forecasts, Reading, UK, 2003.

Langner, J., and H. Rodhe, A Global Three-Dimensional Model of the Tropospheric Sulfur Cycle, *J. Atmos. Chem.*, *13*, 225-263, 1991.

Leaitch, W.R., J.W. Strapp, H.A. Wiebe, and G.A. Isaac, Measurements of Scavenging and Transformation of Aerosol Inside Cumulus, in *Precipitation Scavenging, Dry Deposition and Resuspension*, edited by R.G.S. H.R. Pruppacher, W.G.N. Slinn, pp. 53-69, Elsevier, New York, NY, 1983.

Lelieveld, J., G.-J. Roelofs, L. Ganzeveld, J. Feichter, and H. Rodhe, Terrestrial Sources and Distribution of Atmospheric Sulfur, *Phil. Trans. R. Soc. Lond.*, *352*, 149-158, 1997.

Liss, P.S., and L. Merlivat, Air-Sea Gas Exchange Rates: Introduction and Synthesis, in *The Rate of Air-Sea Exchange in Geochemical Cycling*, edited by P. Buat-Menard, pp. 113-127, D. Reidel Publishing Company, Dordrecht, 1986.

Lohmann, U., R. Leaitch, L.Barrie, K. Law, Y. Yi, D. Bergman, C. Bridgeman, M. Chin, J. Christensen, R. Easter, J. Feichter, A. Jeuken, E.Kjellstroem, D. Koch, C. Land, P. Rasch, and G.-J. Roelofs, Vertical Distributions of Sulfur Species Simulated by Large Scale Atmospheric Models in COSAM: Comparison with Observations, *Tellus B*, *53B*, 646-672, 2001.

Louis, J.-F., A Parameteric Model of Vertical Eddy Fluxes in the Atmosphere, *Boundary Layer Meteorol.*, *17*, 187-202, 1979.

Mather, T.A., D.M. Pyle, and C. Oppenheimer, Tropospheric Volcanic Aerosol, in *Volcanism and the Earth's Atmosphere*, edited by A.R.a.C. Oppenheimer, pp. 189-212, American Geophysical Union, Washington, DC, 2003.

McNair, L.A., R.A. Harley, and A.G. Russell, Spatial Inhomogeneity in Pollutant Concentrations, and their Implications for Air Quality Model Evaluation, *Atmos. Environ.*, *30* (24), 4291-4301, 1996.

Mullen, S.L., and R. Buizza, Quantitative Precipitation Forecasts over the United States by the ECMWF Ensemble Prediction System, *Mon. Weather Rev.*, *129* (4), 638-663, 2001.

Müller, J.F., Geographical Distribution and Seasonal Variation of Surface Emissions and Deposition Velocities of Atmospheric Trace Gases, *J. Geophys. Res.*, *97*, 3787-3804, 1992.

Müller, J.-F., and G. Brasseur, IMAGES: A Three-Dimensional Chemical Transport Model of the Global Troposphere, *J. Geophys. Res.*, *100* (D8), 16445-16490, 1995.

NASA, Chemical Kinetics and Photochemical Data for Use in Stratospheric Modeling. Evaluation #12., pp. 266, National Aeronautics and Space Administration, Jet Propulsion Laboratory, Pasadena, 1997.

National Research Council Panel on Aerosol Radiative Forcing and Climate, A Plan for a Research Program on Aerosol Radiative Forcing and Climate Change, edited by J. Seinfeld, National Academy Press, Washington, DC, 1996.

Olivier, J.G.J., and J.J.M. Berdowski, Global emissions sources and sinks, in *The Climate System*, edited by J. Berdowski, R. Guicherit, and B.J. Heij, pp. 33-78, A.A. Balkema Publishers/Swets & Zeitlinger Publishers, Lisse, The Netherlands, 2001.

Olivier, J.G.J., A.F. Bouwman, C.W.M.v.d. Maas, J.J.M. Berdowski, C. Veldt, J.P.J. Bloos, A.J.H. Visschekijk, P.Y.J. Zandveld, and J.L. Haverlag, Description of EDGAR Version 2: A Set of Global Emissions Inventories of Greenhouse Gases and Ozone-Depleting Substances for all Anthropogenic and Most Natural Sources on a Per Country Basis and on 1^{o} x 1^{o} grid, National Institute of Public Health and Environment, Bilthoven, The Netherlands, 1996.

Olivier, J.G.J., J.A.H.W. Peters, J. Bakker, J.J.M. Berdowski, A.J.H. Visschedijk, and J.P.J. Bloos, Applications of EDGAR: Emissions Database for Global Atmospheric Research, pp. 151, National Institute for Public Health and the Environment (RIVM)/Netherlands Organization for Applied Scientific Research (TNO), Bilthoven, The Netherlands, 2002.

Overton, J.H., Validation of the Hoffmann and Edwards' S(IV)-H_2O_2 Mechanism, *Atmos. Environ.*, *19* (4), 687-690, 1985.

Pasquill, F., The Dispersion of Material in the Atmospheric Boundary Layer - the Basis for Generalization, in *Lectures on Air Pollution and Environmental Impact Analyses*, edited by D.A. Haugen, pp. 1-34, American Meteorological Society, Boston, MA, 1976.

Penner, J., M. Andreae, H. Annegarn, L. Barrie, J. Feichter, D. Hegg, A. Jayraman, R. Leaitch, D. Murphy, J. Nganga, and G. Pitari, Aerosols, their Direct and Indirect Effects, in *Climate Change 2001: The Scientific Basis*, edited by J.T. Houghton, Y. Din, D.J. Griggs, M. Noguer, P.J.v.d. Linden, X. Dai, K. Maskell, and C.A. Johnson, pp. 289-348, Cambridge University Press, Cambridge, UK, 2001.

Pickering, K.E., Y. Wang, W.-K. Tao, C. Price, and J.-F. Müller, Vertical distributions of lightning NOx for use in regional and global chemical transport models, *J. Geophys. Res.. 103*, 31,03– 31216, 1998.

Prasad, V., Y. Kant, P.K. Gupta, C. Elvidge, and K.V.S. Badarinath, Biomass burning and related trace gas emissions from tropical dry deciduous forests of India: A study using DMSP-OLS data and ground-based measurements, *International Journal of Remote Sensing*, *23* (14), 2837-2851, 2002.

Price, C., J. Penner, and M. Prather, NO_x from Lightning 1. Global Distribution Based on Lightning Physics, *J. Geophys. Res.*, *102* (D5), 5929-5941, 1997.

Prospero, J.M., Long-Term Measurements of the Transport of African Mineral Dust to the Southeastern United States: Implications for Regional Air Quality, *J. Geophys. Res.*, *104* (D13), 15917-15927, 1999.

Raes, F., T. Bates, F. McGovern, and M.V. Liedekerke, The 2nd Aerosol Characterization Experiment (ACE-2): General Overview and Main Results, *Tellus*, *52B*, 111-125, 2000.

Ramaswamy, V., O. Boucher, J. Haigh, D. Hauglustaine, J. Haywood, G. Myhre, T. Nakajima, G.Y. Shi, and S. Solomon, Radiative Forcing of Climate Change, in *Climate Change 2001: The Scientific Basis*, edited by J.T. Houghton, Y. Din, D.J. Griggs, M. Noguer, P.J.v.d. Linden, X. Dai, K. Maskell, and C.A. Johnson, pp. 349-416, Cambridge University Press, Cambridge, UK, 2001.

Rasch, P.J., M.C. Barth, J.T. Kiehl, S.E. Schwartz, and C.M. Benkovitz, A Description of the Global Sulfur Cycle and Its Controlling Processes in NCAR CCM3., *J. Geophys. Res.*, *105* (D1), 1367-1385, 2000a.

Rasch, P.J., J. Feichter, K. Law, N. Mahowald, J. Penner, C. Benkovitz, C. Genthon, C. Giannakopoulos, P. Kasibhatla, D. Koch, H. Levy, T. Maki, M. Prather, D.L. Roberts, G.J. Roelofs, D. Stevenson, Z. Stockwell, S. Taguchi, M. Kritz, M. Chipperfield, D. Baldocchi, P. McMurray, L.Barrie, Y. Balkanski, R. Chatfield, E. Kjellstrom, M. Lawrence, H.N. Lee, J. Lelieveld, K.J. Noone, J. Seinfeld, G. Stenchikov, S. Schwartz, C. Walcek, and D. Williamson, A Comparison of Scavenging and Deposition Processes in Global Models: Results from the WCRP Cambridge Workshop of 1995, *Tellus*, *52B*, 1025-1056, 2000b.

Ro, C.U., and R.J. Vet, Analyzed data fields from the National Atmospheric Chemistry Database (NAtChem) and Analysis Facility, Air Quality Research Branch, Meteorological Service of Canada, Environment Canada, Toronto, Ontario, 2002.

Roelofs, G.J., P. Kasibhatla, L. Barrie, D. Bergmann, B. C, M. Chin, J. Christensen, R. Easter, J. Feichter, A. Jeuken, E. Kjellström, D. Koch, C. Land, U. Lohmann, and P. Rasch, Analysis of regional budgets of sulfur species modeled for the COSAM exercise, *Tellus B*, *53B*, 673-694, 2001.

Roelofs, G.-J., and J. Lelieveld, Distribution and Budget of O_3 in the Troposphere Calculated with a Chemistry General Circulation Model, *J. Geophys. Res.*, *100* (D10), 20983-209981, 1995.

Roelofs, G.-J., J. Lelieveld, and L. Ganzeveld, Simulation of Global Sulfate Distribution and the Influence on Effective Cloud Drop Radii with a Coupled Photochemistry-Sulfur Cycle Model, *Tellus*, *50B*, 224-242, 1998.

Schwartz, S.E., Mass-Transport Limitation to the Rate of In-Cloud Oxidation of SO_2: Re-Examination in the Light of New Data, *Atmos. Environ.*, *22* (11), 2491-2499, 1988.

Sheih, C.M., M.L. Wesely, and C.J. Walcek, A Dry Deposition Module for Regional Acid Deposition, U.S. Environmental Protection Agency, Research Triangle Park, NC, 1986.

Spiro, P.A., D.J. Jacob, and J.A. Logan, Global Inventory of Sulfur Emissions with a 1° x 1° Resolution, *J. Geophys. Res.*, *97* (D5), 6023-6036, 1992.

Stockwell, W.R., ON the $HO_2 + HO_2$ Reation: Its Misapplication in Atmospheric Chemistry Models, *J. Geophys. Res.*, *100* (D6), 11695-11698, 1995.

Streets, D.G., N.Y. Tsai, H. Akimoto, and K. Oka, Sulfur Dioxide Emissions in Asia in the Period 1985-1997, *Atmos. Environ.*, *34*, 4413-4424, 2000.

Streets, D.G., N.Y. Tsai, H. Akimoto, and K. Oka, Trends in Emissions of Acidifying Species in Asia, 1985-1997, *Water, Air & Soil Pollu.*, *130*, 187-192, 2001.

Talbot, R.W., R.C. Harriss, E.V. Browell, G.L. Gregory, E.I. Sebacher, and S.M. Beck, Distribution and geochemistry of aerosols in the tropical North Atlantic troposphere: Relationship to Saharan dust, *J. Geophys. Res.*, *91*, 5173-5182, 1986.

ten Brink, H.M., S.E. Schwartz, and P.H. Daum, Efficient Scavenging of Aerosol Sulfate by Liquid-Water Clouds, *Atmos. Environ.*, *21*, 2035-2052, 1987.

U. S. Environmental Protection Agency, National Air Quality and Emissions Trends Report, 1999, pp. 237, U. S. Environmental Protection Agency, Office of Air Quality Planning and Standards, Research Triangle Park, NC, 2001.

U.S Environmental Protection Agency, National Air Pollutant Emission Trends: 1900-1998, U.S. Environmental Protection Agency, Research Triangle Park, NC, 2000.

Uttal, T., J.A. Curry, M.G. Mcphee, D.K. Perovich, R.E. Moritz, J.A. Maslanik, P.S. Guest, H.L. Stern, J.A. Moore, R. Turenne, A. Heiberg, M.C. Serreze, D.P. Wylie, O.G. Persson, C.A. Paulson, C. Halle, J.H. Morison, P.A. Wheeler, A. Makshtas, H. Welch, M.D. Shupe, J.M. Intrieri, K. Stamnes, R.W. Lindsey, R. Pinkel, W.S. Pegau, T.P. Stanton, and T.C. Grenfeld, Surface Heat Budget of the Arctic Ocean, *Bulletin of the American Meteorological Society*, *83* (2), 255-276, 2002.

Vedal, S., Ambient Particles and Health: Lines That Divide, *J. Air Waste Manage. Assoc.*, *47* (5), 551-558, 1997.

Vestreng, V., and H. Klein, Emission Data Reported to UNECE/EMEP: Quality Assurance and Trends Analysis, pp. 101, Meteorological Synthesizing Centre - West, Oslo, Norway, 2002.

Wesely, M., Parameterization of Surface Resistances to Gaseous Dry Deposition in Regional-Scale Numerical Models, *Atmos. Environ.*, *23*, 1293-1304, 1989.

Wooster, M.J., and N. Strub, Study of the 1997 Borneo fires: Quantitative analysis using global area coverage (GAC) satellite data, *Global Biogeochemical Cycles*, *16* (1), doi:1009, 2002.

Wotawa, G., and M. Trainer, The Influence of Canadian Forest Fires on Pollutant Concentrations in the United States, *Science*, *288* (14 April 2000), 324-328, 2000.

Yienger, J.J., and H. Levy, Empirical Model of Global Soil-Biogenic NO_x Emissions, *J. Geophys. Res.*, *100* (D6), 11447-11464, doi:10.1029/97JD00370, 1995.

Table 1. Sulfur species defined in the model.

Species →	**SO_2**		**Sulfate**			**DMS**	**MSA**
Source ↓	**Primary**	**Gas-Phase Oxidation**	**Primary**	**Gas-Phase Oxidation**	**Aq-Phase Oxidation**	**Primary**	**Gas-Phase Oxidation**
North America Anthropogenic 140°W to 30°W	X		X	X	X		
Europe Anthropogenic 30°W to 60°E	X		X	X	X		
Asia Anthropogenic 60°E to 140°W	X		X	X	X		
Volcanic	X			X	X		
Biogenic		X		X	X	X	X
External	X		X	X	X		

Table 2. Input data used in the model and their provenance.

Quantity	Provenance
Meteorology	
2-D Fields	
Cloud base	Based on ECMWF data
Cloud top	Based on ECMWF data
Low, medium and high cloud cover	ECMWF
Stratiform cloud cover	ECMWF
Total cloud cover	ECMWF
Convective precipitation	ECMWF
Stratiform precipitation	ECMWF
Surface pressure	ECMWF
Surface temperature	ECMWF
Solar zenith angle	Calculated based on location and time
SO_2, sulfate, & H_2O_2 dry deposition velocities	Wesely [a]
3-D Fields	
Geopotential	Based on ECMWF algorithm
Cloud liquid water content	ECMWF
Convective cloud mixing fraction	Based on ECMWF data
Air density	Based on ECMWF data
Specific humidity	ECMWF
u- and *v*-components of wind	ECMWF
Vertical velocity ($d\eta/dt$)	Based on ECMWF algorithm
Temperature	ECMWF
Pressure	Based on ECMWF algorithm
Vertical diffusivity coefficient (K_{zz})	Calculated, Section 2.1.1
Oxidant Concentrations	
3-D Fields	
OH, H_2O_2, O_3, HO_2 mixing ratios	MOZART [b]
Emissions	
2-D Fields	
Oceanic DMS	Calculated from surface ocean DMS [c]
Land DMS	Lamb [d]
3-D Fields	
Anthropogenic SO_2 & primary sulfate	EDGAR V3.2 [e]
Volcanic SO_2	Calculated, Section 2.4.3.

[a] Calculated according to Wesely [*Sheih et al.*, 1986; *Wesely*, 1989]; [*Benkovitz et al.*, 1994].

[b] June-July averages from MOZART Version 2 model [*Horowitz et al.*, 2003].

[c] Calculated using [*Kettle et al.*, 1999] and ACE-2 measurements, Section 2.4.2 and Appendix.
[d] Calculated using methodology by B. Lamb [in *Bates et al.*, 1992], Section 2.4.2.
[e] Based on EDGAR Version 3.2 [*Olivier et al.*, 2002] and GEIA 1985 [*Benkovitz et al.*, 1996].

Table 3. Information on volcano emissions used in the model. Emissions are totals for the simulation period (June 1 to July 24, 1997).

Volcano	Latitude	Longitude	Height‡ (km)	Emissions (Gg S)	Country	Method	Data
Popocatepetl	19.02	-98.62	5.5	259	Mexico	M	(a)
Etna	37.73	15.00	3.4	110	Sicily, Italy	M	(b)
Ruiz	4.90	-75.32	5.3	52.2	Columbia	A	(e)
Sakura-Jima	31.58	130.67	1.1	52.2	Japan	A	(e)
Pu`uO`O *	19.45	-155.29	0.76	42.5	Hawaii, USA	M	(f)
Soufrière Hills	16.70	-62.20	0.92	22.4	Montserrat Island	M	(c)
Masaya	11.98	-86.16	0.64	21.7	Nicaragua	A	(e)
Satsuma Iwojima (Kikai)	30.78	130.28	0.72	20.4	Japan	R	(e)
Galeras	1.22	-77.37	4.3	17.9	Columbia	A	(e)
Fuego	14.47	-90.88	3.8	17.6	Guatemala	A	(e)
SanCristobal	12.70	-87.00	1.7	16.2	Nicaragua	A	(e)
Mayon	13.26	123.69	2.5	14.6	Philippines	A	(e)
Pacaya	14.38	-90.60	2.6	14.0	Guatemala	A	(e)
Poas	10.20	-84.23	2.7	13.8	Costa Rica	A	(e)
Asama	36.40	138.53	2.6	10.2	Japan	A	(e)
Bulusan	12.77	124.05	1.6	10.2	Philippines	A	(e)
Oshima	34.73	139.38	0.76	7.4	Japan	A	(e)
Santa Maria	14.76	-91.55	3.8	6.3	Guatemala	A	(e)
Karumsky	54.05	159.43	1.5	4.9	Kamchatka, Russia	A	(d)
Kuju	33.08	131.25	1.8	3.8	Japan	A	(e)
Stromboli	38.79	15.21	0.93	3.7	Aeolian Islands, Italy	M	(a)
Unzen	32.75	130.30	1.4	3.6	Japan	A	(e)
Arenal	10.46	-84.70	1.7	3.0	Costa Rica	A	(e)
Bezymianny	55.98	160.59	2.9	2.8	Kamchatka, Russia	A	(d)
Halemaumau†	19.45	-155.29	1.2	2.5	Hawaii, USA	M	(f)
Telica	12.60	-86.85	1.1	2.3	Nicaragua	A	(e)
Aso	32.88	131.10	1.6	2.1	Japan	A	(e)
Momotobo	12.42	-86.54	1.3	2.0	Nicaragua	A	(e)
Medvezhia	45.38	148.83	1.1	1.9	Kurile Islands, Russia	A	(e)
Usu	42.53	140.83	0.73	1.5	Japan	A	(e)
Sheveluch	56.65	161.35	2.8	1.4	Russia	A	(d)
Augustine	59.38	-153.42	1.3	1.3	Alaska, USA	A	(e)
Iliamna	60.03	-153.08	3.1	0.61	Alaska, USA	A	(e)

Volcano	Latitude	Longitude	Height‡ (km)	Emissions (Gg S)	Country	Method	Data
Erta Ale	13.60	40.67	0.61	0.59	Ethiopia	A	(e)
Santa Ana	13.85	-89.63	2.4	0.55	El Salvador	A	(e)
Izalco	13.81	-89.63	2.0	0.55	El Salvador	A	(e)
Vulcano	38.4	14.96	0.5	0.37	Aeolian Islands, Italy	M	(b)
Kverkfjoll	64.65	-16.72	1.9	0.082	Iceland	A	(e)
Martin	58.17	-155.35	1.9	0.082	Alaska, USA	A	(e)
Total				749			

‡ Height of volcano cone.

* Vent of Kilauea volcano, Hawaii, USA.

† Main crater of Kilauea volcano, Hawaii, USA.

Method

M = measurements for some days, linear interpolation for days with no measurements.

R = range of emissions. Random number used to generate daily emissions.

A = constant 25-yr average degassing (e).

Data

(a) H. Delgado, Universidad Nacional Autónoma de México, Coyoacán, Mexico, personal communication, 1999.

(b) T. Caltabiano, Istituto Internazionale di Vulcanologia, Catania, Italy, personal communication, 1999.

(c) P. Francis (deceased), Open University, Milton Keynes, UK, personal communication, 1998.

(d) P. Kyle, New Mexico Institute of Mining and Technology, NM, USA, personal communication, 1999.

(e) [*Andres and Kasgnoc*, 1998]

(f) [*Elias et al.*, 1998]

Table 4. Contributions of source regions and source types to sulfur emissions and burdens.

Source Region	Emissions (Tg S)			Burden[†] Sulfate		Burden[†] SO_2	
	8-Week[*]	Year[§]	(%)	Gg S	(%)	Gg S	(%)
All sources	11.2	73		597		197	
Anthropogenic	9.0	58	80	502	84	160	81
North America	1.9	12	17	92	15	28	14
Europe	3.0	20	27	193	32	64	33
Asia	4.1	27	36	218	37	68	34
Volcanic	0.7	5	7	63	10	27	14
Biogenic	1.5	10	13	32	5	10	5

[*] Total emissions for the 8-week simulation period.
[§] Emissions extended to year to facilitate comparison with other studies.
[†] Average over 6-week analysis period.

Table 5. Information on the measurements used to evaluate model results.

Network Area	Number Stat	Number Obs	Measurements	Sampling Intervals	Data Provider	% Obs
ACE-2 [k]	2	57	SO_2 (several)[*]	Semi-		0.2
Short term	7	183	Sulfate (several)[*]	continuous	IGAC [§]	3.0
ABPM [l]						
Canada	7	14	Wet Dep	Twice month	Nat/Chem [‡]	0.6
AEROCE [a]						
Oceanic	4	116	Sulfate (24-h)	Every day	D. Savoie [s]	1.9
AIRMoN [i]	8	34	Sulfate	Every week		0.6
US	9	76	Wet Dep	Every week	Nat/Chem [‡]	3.2
AIRS [b]	597	16655	SO_2 (1-h) [*]	Continuous	V. Ambrose [t]	68.8
US	192	1334	Sulfate (24-h)	Every 6th day		22.0
BCPCSN [m]						
Canada	4	15	Wet Dep	Every week	Nat/Chem [‡]	0.6
CAPMoN [c]	10	332	SO_2 (24-h)	Every day	Nat/Chem [‡]	1.4
Canada	10	352	Sulfate (24-h)	Every day		5.8
	21	340	Wet Dep	Every day		14.4
CASTNet [d]	69	330	SO_2 (7 days)	Every week	Nat/Chem [‡]	1.4
US	67	327	Sulfate (7 days)	Every week		5.4
	19	78	Wet Dep	Every week		3.3
EMEP [e]	82	2511	SO_2 (24-h)	Every day	A.-G. Hjellbrekke [u]	10.4
Europe	78	2805	Sulfate (24-h)	Every day		46.2
	77	924	Wet Dep	Event		39.0
GAViM [f]						
Canada	3	33	Sulfate (24-h)	Every 3rd day	Nat/Chem [‡]	0.5
IMPROVE [g]	7	67	SO_2 (24-h)	2 days/week	K. Perry [v]	0.3
US	64	647	Sulfate (24-h)	2 days/week		10.7
NADP [n]						
US	179	681	Wet Dep	Weekly	NADP web site [†]	28.8
NAPS [j]	55	1635	SO_2 (24-h)	Every day	Nat/Chem [‡]	6.8
Canada	32	160	Sulfate (24-h)	Every 6th day		2.6
NBPMN [o]						
Canada	13	61	Wet Dep	Every week	Nat/Chem [‡]	2.6
NEPMoN [p]						
Canada	2	8	Wet Dep	Every week		0.3
NSPSN [q]						
Canada	1	15	Wet Dep	Every day	Nat/Chem [‡]	0.6
NYST [h]	2	59	SO_2 (24-h)	Every day	L. Husain [w]	0.2
US	2	64	Sulfate (24-h)	Every day		1.0

Network Area	Number Stat	Obs	Measurements	Sampling Intervals	Data Provider	% Obs
REPQ [r] Canada	37	154	Wet Dep	Weekly	Nat/Chem [‡]	6.5
Cheju	1	38	SO_2 (1-h) [*]	Continuous	Y.P. Kim [x]	0.2
Island	1	12	Sulfate (48-h)	Every 3rd	C.H. Kang [y]	0.2
Korea				day		
Taiwan	69	2509	SO_2 (1-h) [*]	Continuous	C.M. Liu [z]	10.4

[*] Measurements averaged to 24-h for comparison with observations.

[a] Aerosol Oceanic Chemistry Experiment
[b] Aerometric Information Retrieval System
[c] Canadian Air and Precipitation Monitoring Network.
[d] Clean Air Status and Trends Network.
[e] European Modeling and Evaluation Programme Network.
[f] Guelph Aerosol and Visibility Monitoring Program.
[g] Interagency Monitoring of Protected Visual Environments.
[h] New York State Department of Health stations at Whiteface Mountain and Mayville, NY.
[i] Atmospheric Integrated Research Monitoring Network.
[j] National Air Pollution Surveillance Network.
[k] Aerosol Characterization Experiment (ACE)-2.
[l] Alberta Precipitation Monitoring Network.
[m] British Columbia Precipitation Chemistry Sampling Network.
[n] National Atmospheric Deposition Network.
[o] New Brunswick Precipitation Monitoring Network.
[p] Newfoundland Acid Precipitation Monitoring Network.
[q] Nova Scotia Precipitation Study Network.
[r] Reseau d'Echantillonnage des Precipitations du Quebec.
[s] University of Miami, Coral Gables, FL, USA.
[t] US Environmental Protection Agency, Research Triangle Park, NC, USA.
[u] Norwegian Institute for Air Research, Kjeller, Norway.
[v] San Jose State University, San Jose, CA, USA.
[w] New York State Department of Health, Albany, NY, USA.
[x] Korea Institute of Science and Technology, Seoul, Korea.
[y] Cheju University, Cheju, Korea.
[z] National Taiwan University, Taipei, Taiwan.
[§] International Global Atmospheric Chemistry Program (IGAC) ACE-2 Data Sets.
[†] http://nadp.sws.uiuc.edu.
[‡] The Canadian National Atmospheric Chemistry (Nat/Chem) Database and Analysis System [*Ro and Vet*, 2002].

Table 6. SO_2 Sinks, Amount of SO_2 in Areas Where the SO_2 Mixing Ratio is Less Than the H_2O_2 Mixing Ratio, and Amount of SO_2 in Cloud by Source Region and Source Type.

Source Region	Sinks (% sources)					F_{aq} (%)	$F^{\dagger}_{SO_2}$ (%)	$F^{\ddagger}_{cl}$ (%)
	Aq-Conv Aerosol	Reactive Rainout	Total Aq-Conv	Gas-Conv	Dry Dep			
All	33	23	56	16	27	67	45	13
NA	32	28	60	13	27	71	56	9
Eu	32	18	50	19	31	63	48	12
As	34	22	56	15	29	69	33	14
Volcanic	34	32	66	30	6	53	40	15
Biogenic	39	29	68	10	22	80	94	12

Aq-Conv Aerosol is the aqueous-phase generated sulfate that contributes to aerosol burden.

Reactive Rainout is the aqueous-phase sulfate generated and deposited in same event.

Total Aq-Conv is the total aqueous-phase conversion (aq-conv aerosol plus reactive rainout).

F_{aq}, the fraction of SO_2 converted to aerosol sulfate by aqueous-phase oxidation, was calculated as the amount of SO_2 converted to aerosol sulfate via aqueous-phase conversion divided by the amount of SO_2 converted to aerosol sulfate via aqueous- and gas-phase conversion.

Wet deposition is less than 0.01% of the SO_2 sinks for all source regions and source types.

† Time- and domain-average fraction of SO_2 located in areas where SO_2 mixing ratios are less than or equal to H_2O_2 mixing ratios (see Section 5 for details).

‡ Time- and domain-average fraction of SO_2 located in clouds with cloud liquid water fraction $\geq 10^{-9}$ (see Section 5 for details).

Table 7. Effective First-order Removal Rates (τ^{-1}) and Turnover Times (τ) for SO_2 and DMS.

Source Region	τ^{-1}, % day^{-1}				τ (days)
	Dry Deposition	OH Conversion	Aqueous Conversion	Total	
All	24	14	51	89	1.1
North America	30	14	67	111	0.9
Europe	25	15	39	79	1.2
Asia	29	14	57	100	1.0
Volcanic	3	13	29	45	2.2
Biogenic SO_2	32	15	102	149	0.7
DMS		99		99	1.0

Table 8. Effective First-order Removal Rates (τ^{-1}) and Turnover Times (τ) for Aerosol Sulfate and MSA, Yields of Aerosol Sulfate (fraction of SO_2 that is oxidized to aerosol sulfate) and MSA (fraction of DMS that is oxidized to MSA), Aerosol Sulfate Burden/Sulfur Sources, Sulfate Sinks, and Amount of Sulfate Encountering Precipitating Clouds.

Source Region	τ^{-1} (% day^{-1})			τ (days)	Aerosol Yield, %	Sulfate (or MSA) Potential (days)	Sinks (% Total)		$F_{cl}^{\ddagger}$ (%)
	Dry Dep	Wet Dep	Total				Wet Dep	Dry Dep	
All	1.6	13	15	6.9	50	3.4	89	11	10.7
North America	1.7	14	15	6.5	45	2.9	89	11	10.9
Europe	2.0	11	13	7.9	50	3.7	84	16	9.0
Asia	1.4	14	15	6.4	49	3.2	91	9	11.9
Volcanic	1.0	10	11	9.0	64	5.2	92	8	8.7
Biogenic: SO_4	2.2	21	23	4.3	49	2.2	91	9	15.9
MSA	3.3	22	25	3.9	11	0.3	87	13	

Sulfate Potential is the sulfate burden divided by the sulfur emissions. Sulfate potential for biogenic sources is the biogenic sulfate burden divided by the biogenic SO_2. MSA potential is MSA burden divided by DMS emissions.

‡ Time- and domain-average fraction of sulfate in precipitating clouds with cloud liquid water fraction $\geq 10^{-9}$ (see Section 5 for details).

Table 9. Models Used for Comparisons of Lifetimes and Sinks of Sulfate and SO_2.

Model	Resolution Vertical Levels	Met Data [a]	Simulation Period [g]	Oxidant Concentrations	Reference
Hamburg ECHAM GCM [b]	5.625°×5.625° 19	GCM	5 years	Prescribed	[*Feichter et al.*, 1996]
Hamburg ECHAM GCM	5.625°×5.625° 19	GCM		[*Roelofs and Lelieveld*, 1995]	[*Lelieveld et al.*, 1997]
Hamburg ECHAM GCM	5.625°×5.625° 19	GCM	3 years	[*Roelofs and Lelieveld*, 1995]	[*Roelofs et al.*, 1998]
GISS GCM II-prime	4°×5° 9	GCM	6 years	Spivakovsky [e], personal comm	[*Koch et al.*, 1999]
NCAR/ CCM3	2.8°×2.8° 18	GCM	7 years	IMAGES [f] [*Müller and Brasseur*, 1995]	[*Rasch et al.*, 2000]
GOCART	2°×2.5° 25	GEOS/DAS [c]	6 years	IMAGES [*Müller and Brasseur*, 1995]	[*Chin et al.*, 2000]
GChM-O Version 1	1.125°×1.125° 15	ECMWF [d]	June-July 1986	Prescribed [h]	[*Benkovitz et al.*, 1994]
GChM-O Version 2	1°×1° 27	ECMWF	June-July 1997	MOZART [i] [*Horowitz et al.*, 2003]	This study

[a] Meteorological data source.
[b] General Circulation Model.
[c] Goddard Earth Observing System/Data Assimilation System. Cloud fraction and cloud water content derived from empirical formulations.
[d] European Centre for Medium-Range Weather Forecasts.
[e] C. Spivakovsky, Harvard University, Cambridge, MA.
[f] Intermediate Model of Global Evolution of Species.
[g] Number of years of simulation; results were reported as averages for those years.
[h] H_2O_2 generated at fixed rate dependant on season. OH from C. Spivakovsky, Harvard University, Cambridge, MA, personal communication.
[I] Model of Ozone and Related Chemical Tracers.

Table 10. Sink rates, inverse lifetimes, lifetimes, contributions to sinks, burden of SO_2 and sulfate, and sulfate potential from this study and other models.

	F96	L97	R98	K99	R00	C00	B97	This Study
Sink Rates (%/day)								
SO_2								
Dry Deposition	26	10	8	17	16	26	12	24
Wet Deposition	5	0	0	0	1	7	0	4×10^{-4}
Gas Conversion	11	7	8	6	6	9	8	14
Aqueous Conversion to sulfate	22	26	27	15	29	15	16	30[a]
Oxidation & immediate wet deposition								21
Sulfate								
Dry Deposition	3	5	5	4	2	2	3	2
Wet Deposition	20	14	17	14	23	15	18	13
Inverse Lifetime (%/day)								
SO_2	63	43	42	38	53	56	36	90
Sulfate	23	19	21	18	25	17	21	15
DMS	48	200		53	71	50	34	100
MSA				13		14	21	25
Lifetime (days)								
SO_2	1.6	2.3	2.4	2.6	1.9	1.8	2.8	1.1
Sulfate	4.4	5.3	4.7	5.7	4.0	5.8	4.7	7.0[a]
DMS	2.1	0.5		1.9	1.4	2.0	2.9	1.0
MSA				7.6		7.1	4.8	3.9
Sinks (%)								
SO_2								
Dry Deposition	42	24	18	44	31	46	34	27
Wet Deposition	8	0	0	0.2	2	12	< 1	4×10^{-4}
Gas Conversion	17	16	18	16	12	16	21	16
Aqueous Conversion	34	59	64	39	56	27	45	56[b]
Sulfate								
Dry Deposition	14	25	22	20	7	13	14	11
Wet Deposition	86	75	78	80	93	87	86	89
Sulfate yield, %[c]	51	76	82	55	68	43	66	50
Burden (Tg S)								
SO_2	0.33	0.56	0.61	0.56	0.4	0.43		0.20[d]
Sulfate	0.43	1.05	0.96	0.73	0.60	0.63		0.60[d]
Sulfate Potential (days)[e]	2.1	4.4	3.7	3.4	2.5	2.7		3.3

[a] Includes aerosol sulfate only, ie, does not include sulfate generated and removed in the same time step.

[b] Includes 33% conversion to aerosol sulfate and 23% sulfate generated and removed in the same time step.

[c] Calculated as chemical conversion rate of SO_2/sink rate of SO_2.

[d] Covers only model domain; average over 6-week analysis period.

[e] Calculated as sulfate burden/(SO_2 burden × SO_2 inverse lifetime).
F96 = [*Feichter et al.*, 1996].
B97 = June-July 1986 simulation, [*Benkovitz et al.*, 1994, *Benkovitz and Schwartz*, 1997].
L97 = [*Lelieveld et al.*, 1997].
R98 = [*Roelofs et al.*, 1998].
K99 = [*Koch et al.*, 1999].
R00 = [*Rasch et al.*, 2000].
C00 = [*Chin et al.*, 2000].

Figure Captions

Figure 1. Schematic of the processes included in the Global Chemistry Model driven by observation-derived meteorology (GChM-O). See Table 2 for the description of the meteorology derived fields. ***Bold oblique*** characters indicate changes in Version 2.

Figure 2. Heights of the mixed layer for June 29, 1997. Note the general increase in height over the oceans from the poles to the tropics, the relatively lower depths over regions of ocean upwelling such as off the coast of California, and the clear diurnal cycle particularly over land (for example, the European continent shows relatively lower height over the entire region at 00UT compared to 12UT).

Figure 3. Fractional incorporation of sulfate into cloud water. This mechanism is activated only when cloud liquid water volume fraction is $> 10^{-9}$. Dashed lines indicate the values of L_{mid} and $0.5f_{max}$ (see Section 2.2.1).

Figure 4. Sulfur emissions for the simulation period: a) anthropogenic sources, b) average biogenic sources, c) average volcanic sources. All panels use the scale shown. Volcanic emissions were divided by the area of the model grid cell where the volcano is located. The vertical lines in a) delimit the anthropogenic source regions distinguished in the model, North America (NA), Europe (Eu), Asia (As). The rectangle delimits the ACE-2 experimental area (25°W to 8°W longitude; 23°N to 44°N latitude).

Figure 5. Map of the evaluation locations for sulfate and SO_2. TS denotes locations for which time series data were available, MO denotes locations at which there were multiple observations.

Figure 6. Time series of the modeled and observed sulfate mixing ratios at the 90 locations that had at least 28 observations for the period June 17 to July 24, 1997. The three numbers, *i,j,k* at the top right of each panel represent the three-dimensional model coordinates of the location. Model domain is numbered east from the prime meridian (0 to 360), north from the equator (0 to 81), and vertical levels are numbered from the surface.

Figure 7. Examples of time series of SO_2 at locations with more than one station. Each horizontal pair of panels represents one model grid cell; the three numbers, *x,y,z*, at the top right of the left panel represent the three-dimensional model coordinates (*i,j,k*) of the location. In all panels the black lines represent the model results. In column a the cityscape red lines represent the average of all the observed mixing ratios. In column b the cityscape lines represent observed mixing ratios at individual stations within the model grid cell; the vertical spread of these lines on a given date represents the within-location spatial variability of the mixing ratios on that date. Note the artificial lower limit for reporting the observed mixing ratios for one station on the last panel.

Figure 8. Scatterplots of modeled vs observed mixing ratios of a) sulfate, and b) SO_2. n indicates the number of cases in each plot. Observed SO_2 MRs in a straight line, especially evident at 1 ppb, were caused by an artificial setting of the lower limit of reporting for measurements; this is further illustrated in Figure 7.

Figure 9. Histograms of the differences between modeled and observed values classified by the values of the observation a) sulfate mixing ratios, b) SO_2 mixing ratios, and c) sulfate concentration in precipitation.

Figure 10. Histograms of the distribution of the ratio characteristic spread. a) characteristic spread of the observed sulfate mixing ratios within individual locations, b) characteristic spread of model and observed sulfate mixing ratios for the data set included in Figure 10a, and c) characteristic spread of all modeled and observed sulfate mixing ratios,.

d) characteristic spread of the observed SO_2 mixing ratios within individual locations, e) characteristic spread of model and observed SO_2 mixing ratios for the data set included in Figure 10d, and

f) characteristic spread of all modeled and observed SO_2 mixing ratios, g) characteristic spread of the observed sulfate concentration in precipitation within individual locations, h) characteristic spread of model and observed sulfate concentration in precipitation for the data set included in Figure 10g, and

i) characteristic spread of all modeled and observed sulfate concentration in precipitation.

Figure 11. Areas where the SO_2 mixing ratios are greater than the H_2O_2 mixing ratios on July 6, 1997 at 00UT for model level number (avg height, m) a) 4 (789), b) 3 (478), c) 2 (232), and d) 1 (65).

Figure C-1. Histogram of the distribution of observations among networks, a) sulfate mixing ratios, b) SO_2 mixing ratios, and c) sulfate concentration in precipitation. Shading denotes fraction of observations for which mixing ratios or concentrations were within the individual ranges.

Figure C-2. Histograms of the distribution of the observed mixing ratios for the data set containing multiple observations within a location and of the whole data set, a) sulfate, and b) SO_2.

Figure 1

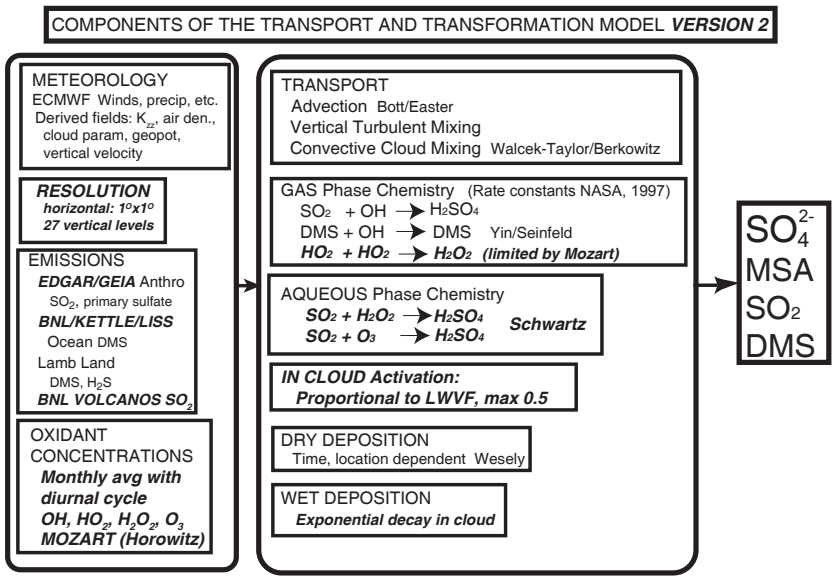
COMPONENTS OF THE TRANSPORT AND TRANSFORMATION MODEL VERSION 2
METEOROLOGY
ECMWF Winds, precip, etc.
Derived fields: K_{zz}, air den., cloud param, geopot, vertical velocity
RESOLUTION
horizontal: 1°x1°
27 vertical levels
EMISSIONS
EDGAR/GEIA Anthro
SO_2, primary sulfate
BNL/KETTLE/LISS
Ocean DMS
Lamb Land
DMS, H_2S
BNL VOLCANOS SO_2
OXIDANT CONCENTRATIONS
Monthly avg with diurnal cycle
OH, HO_2, H_2O_2, O_3
MOZART (Horowitz)
TRANSPORT
Advection Bott/Easter
Vertical Turbulent Mixing
Convective Cloud Mixing Walcek-Taylor/Berkowitz
GAS Phase Chemistry (Rate constants NASA, 1997)
SO_2 + OH → H_2SO_4
DMS + OH → DMS Yin/Seinfeld
HO_2 + HO_2 → H_2O_2 (limited by Mozart)
AQUEOUS Phase Chemistry
$SO_2 + H_2O_2 \rightarrow H_2SO_4$
$SO_2 + O_3 \rightarrow H_2SO_4$
Schwartz
IN CLOUD Activation:
Proportional to LWVF, max 0.5
DRY DEPOSITION
Time, location dependent Wesely
WET DEPOSITION
Exponential decay in cloud
SO_4^{2-}
MSA
SO_2
DMS

Figure 2

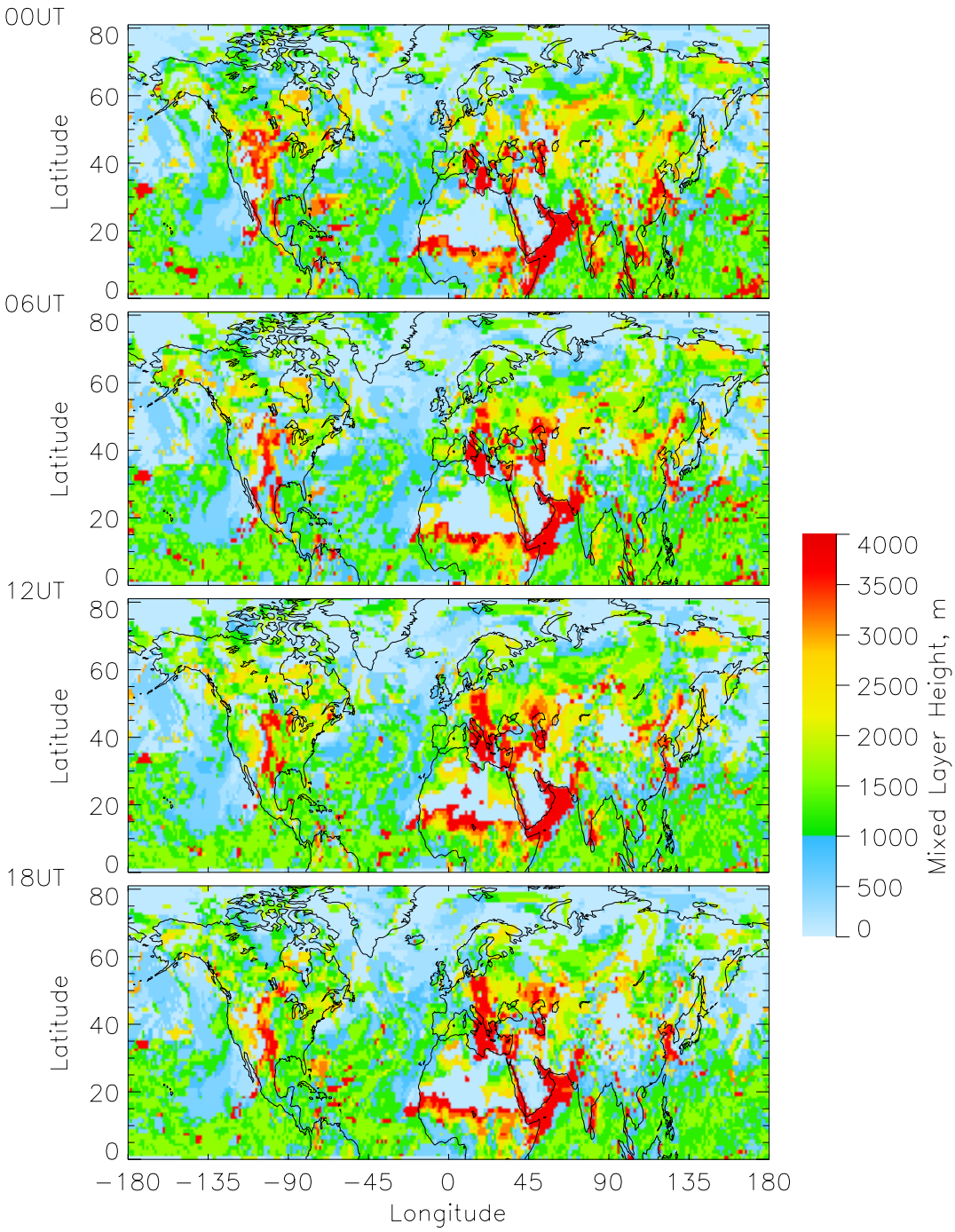
00UT
06UT
12UT
18UT
Latitude
80
60
40
20
0
−180
−135
−90
−45
0
45
90
135
180
Longitude
4000
3500
3000
2500
2000
1500
1000
500
0
Mixed Layer Height, m

Figure 3

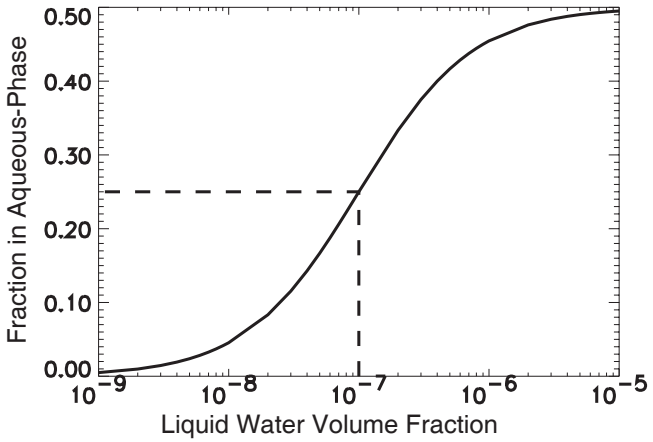
Fraction in Aqueous-Phase
0.50
0.40
0.30
0.20
0.10
0.00
10^-9
10^-8
10^-7
10^-6
10^-5
Liquid Water Volume Fraction

Figure 4

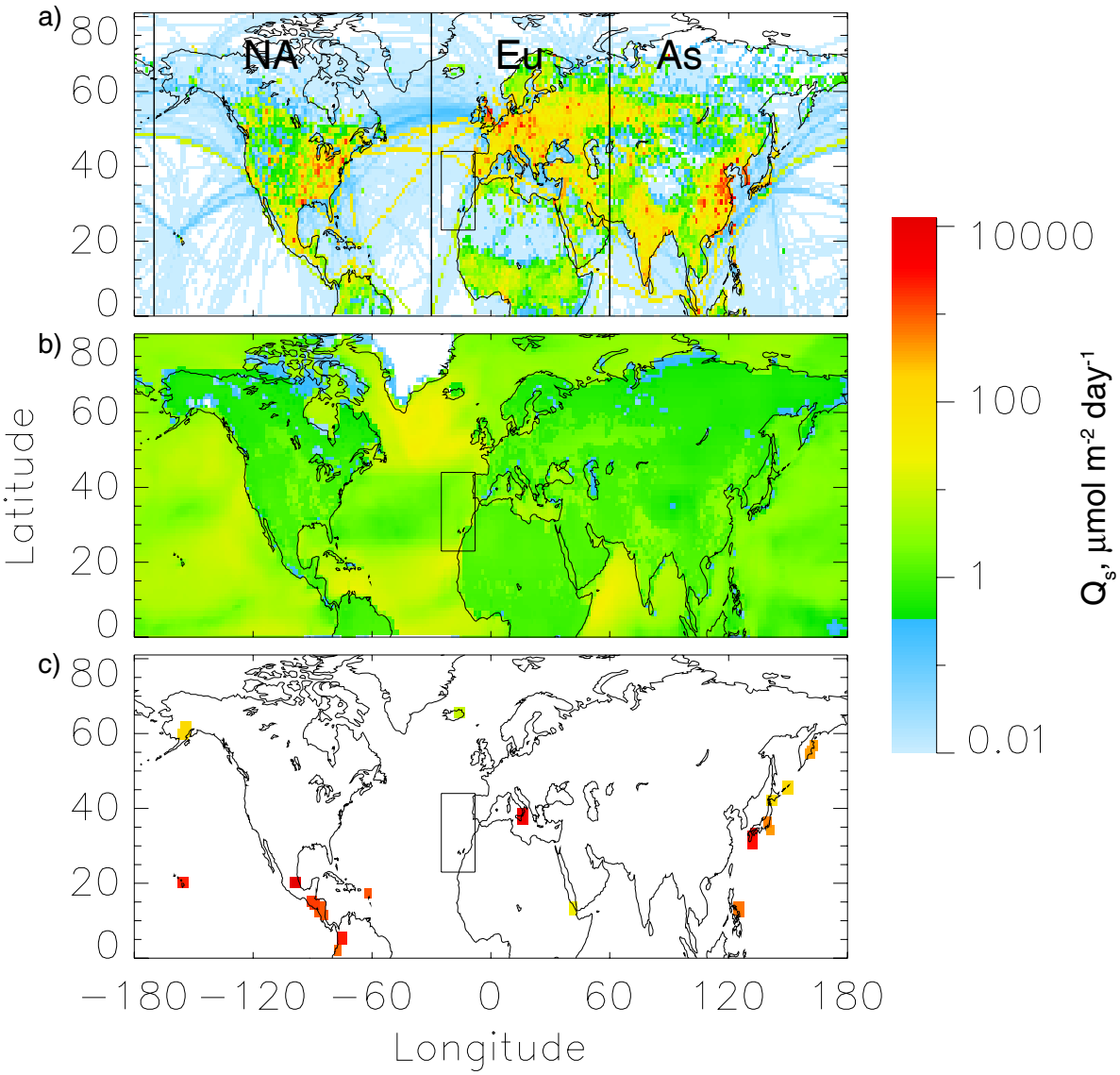
a)
b)
c)
NA
Eu
As
80
60
40
20
0
Latitude
−180
−120
−60
0
60
120
180
Longitude
10000
100
1
0.01
Q_s, µmol m^{-2} day^{-1}

Figure 5

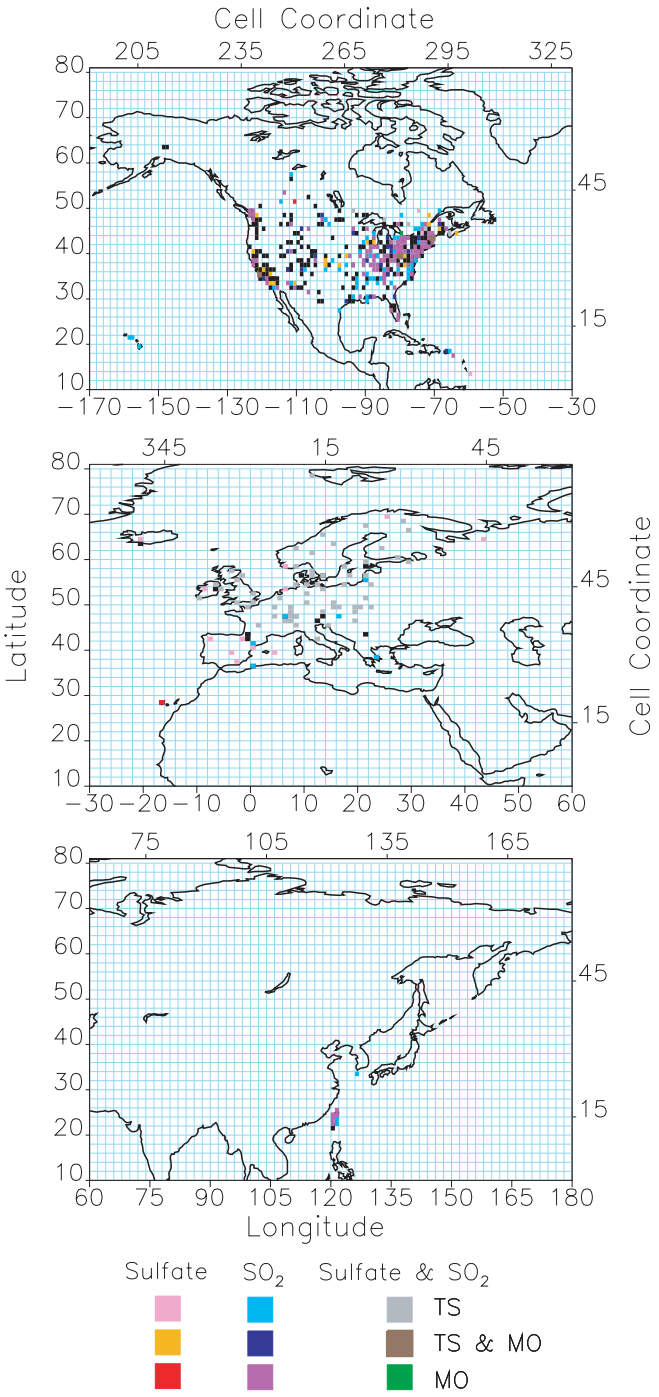
Cell Coordinate
205
235
265
295
325
80
70
60
50
40
30
20
10
45
15
−170 −150 −130 −110 −90 −70 −50 −30
345
15
45
Latitude
Cell Coordinate
−30 −20 −10 0 10 20 30 40 50 60
75
105
135
165
60 75 90 105 120 135 150 165 180
Longitude
Sulfate
SO2
Sulfate & SO2
TS
TS & MO
MO

Figure 6

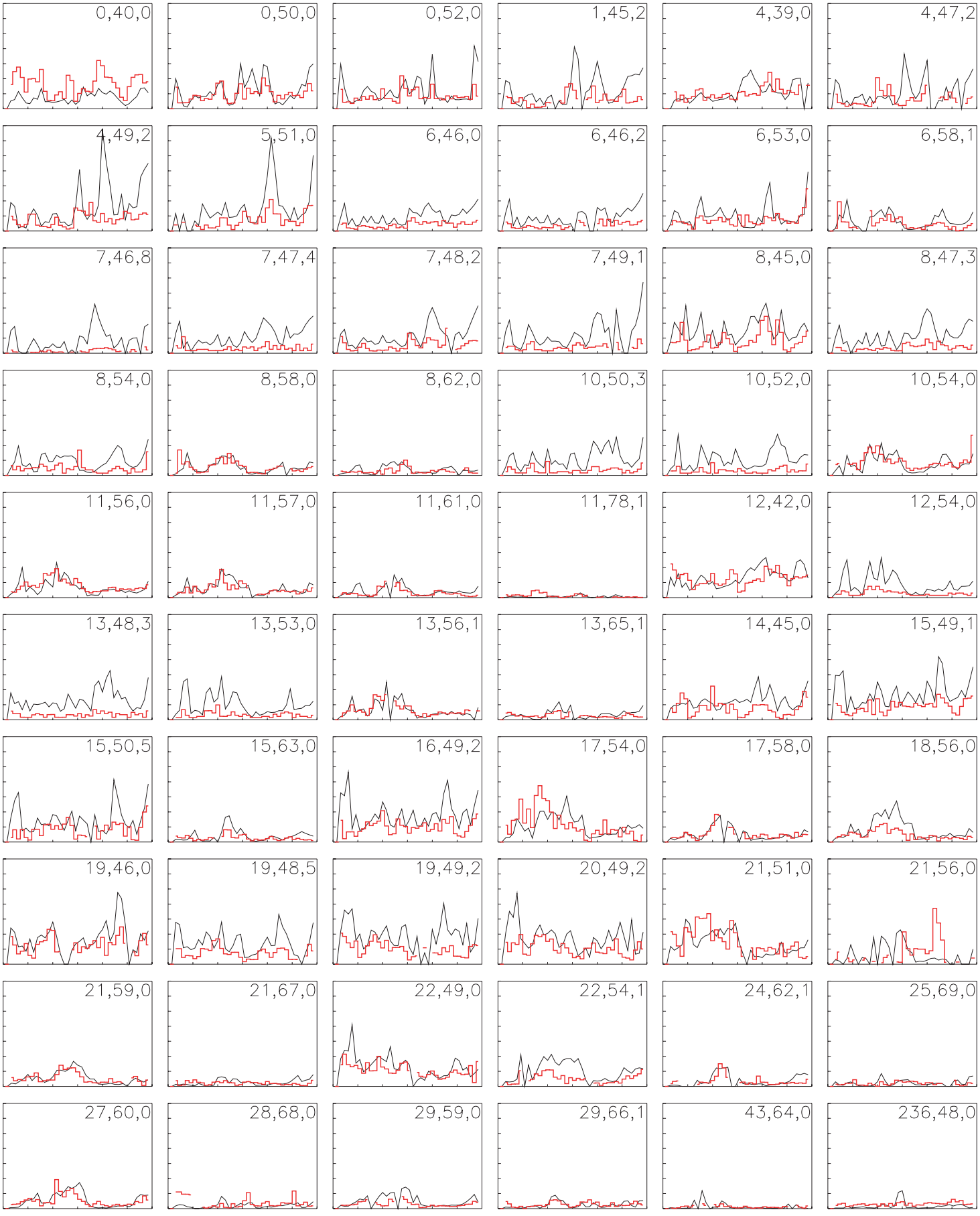
0,40,0
0,50,0
0,52,0
1,45,2
4,39,0
4,47,2
4,49,2
5,51,0
6,46,0
6,46,2
6,53,0
6,58,1
7,46,8
7,47,4
7,48,2
7,49,1
8,45,0
8,47,3
8,54,0
8,58,0
8,62,0
10,50,3
10,52,0
10,54,0
11,56,0
11,57,0
11,61,0
11,78,1
12,42,0
12,54,0
13,48,3
13,53,0
13,56,1
13,65,1
14,45,0
15,49,1
15,50,5
15,63,0
16,49,2
17,54,0
17,58,0
18,56,0
19,46,0
19,48,5
19,49,2
20,49,2
21,51,0
21,56,0
21,59,0
21,67,0
22,49,0
22,54,1
24,62,1
25,69,0
27,60,0
28,68,0
29,59,0
29,66,1
43,64,0
236,48,0

Figure 6, cont'd

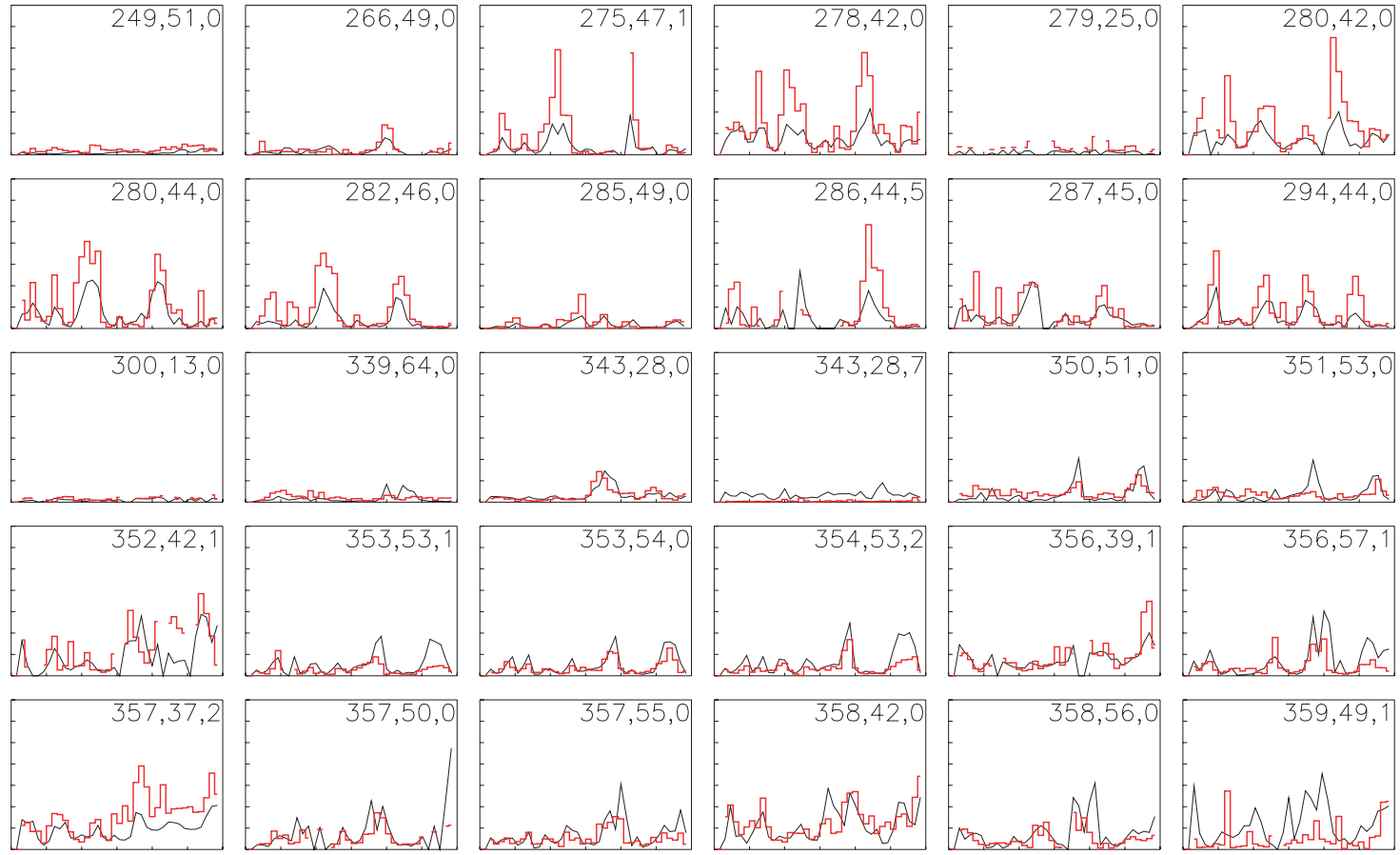

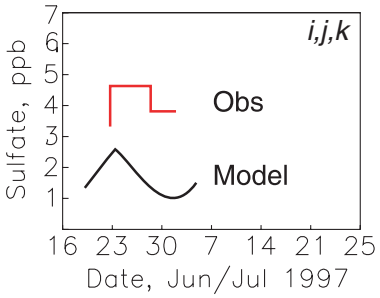

Figure 7

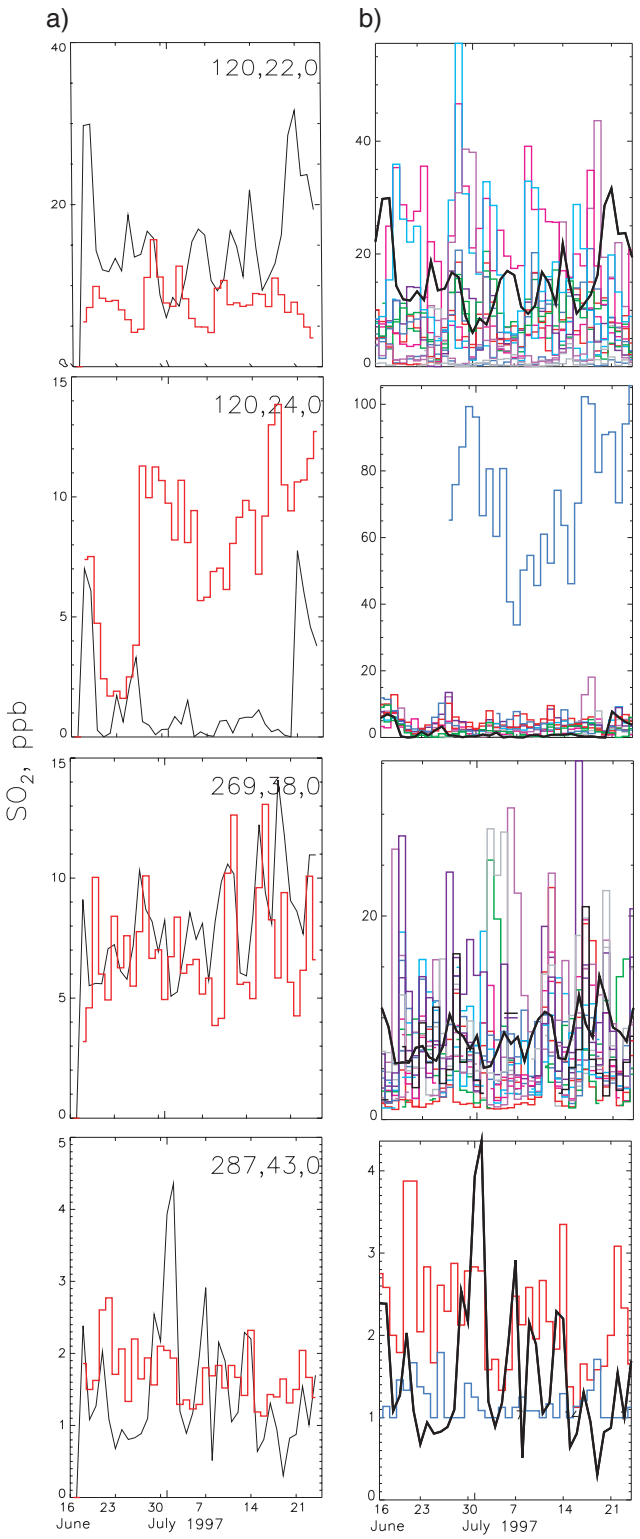
a)
b)
120,22,0
120,24,0
269,38,0
287,43,0
SO_2, ppb
16 23 30 7 14 21
June July 1997

Figure 8

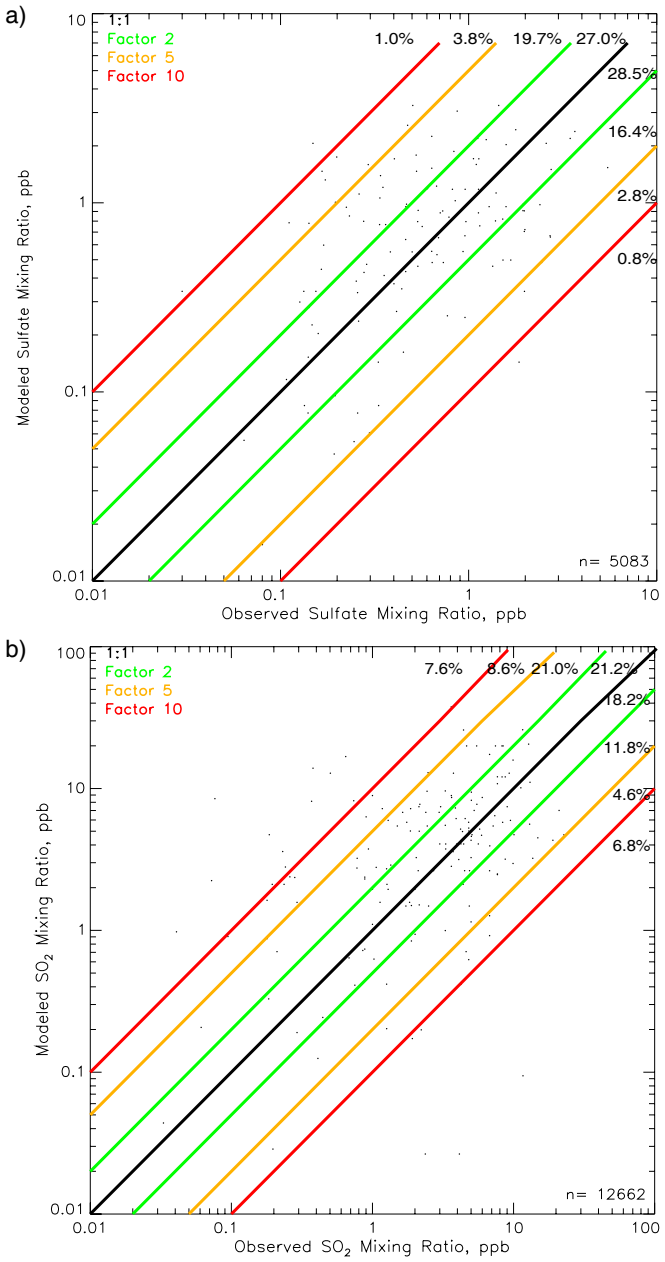
a)
1:1
Factor 2
Factor 5
Factor 10
1.0%
3.8%
19.7%
27.0%
28.5%
16.4%
2.8%
0.8%
n= 5083
Modeled Sulfate Mixing Ratio, ppb
Observed Sulfate Mixing Ratio, ppb
0.01
0.1
1
10
b)
1:1
Factor 2
Factor 5
Factor 10
7.6%
8.6%
21.0%
21.2%
18.2%
11.8%
4.6%
6.8%
n= 12662
Modeled SO2 Mixing Ratio, ppb
Observed SO2 Mixing Ratio, ppb
0.01
0.1
1
10
100

Figure 9

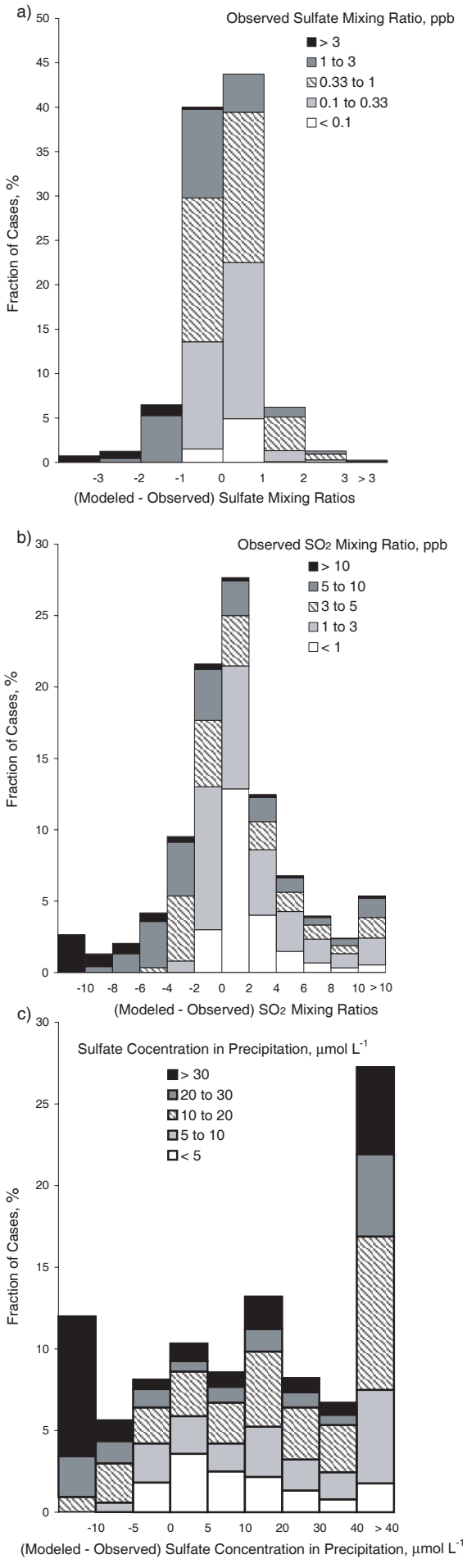
a)
Observed Sulfate Mixing Ratio, ppb
> 3
1 to 3
0.33 to 1
0.1 to 0.33
< 0.1
Fraction of Cases, %
(Modeled - Observed) Sulfate Mixing Ratios
b)
Observed SO2 Mixing Ratio, ppb
> 10
5 to 10
3 to 5
1 to 3
< 1
Fraction of Cases, %
(Modeled - Observed) SO2 Mixing Ratios
c)
Sulfate Cocentration in Precipitation, µmol L-1
> 30
20 to 30
10 to 20
5 to 10
< 5
Fraction of Cases, %
(Modeled - Observed) Sulfate Concentration in Precipitation, µmol L-1

Figure 10

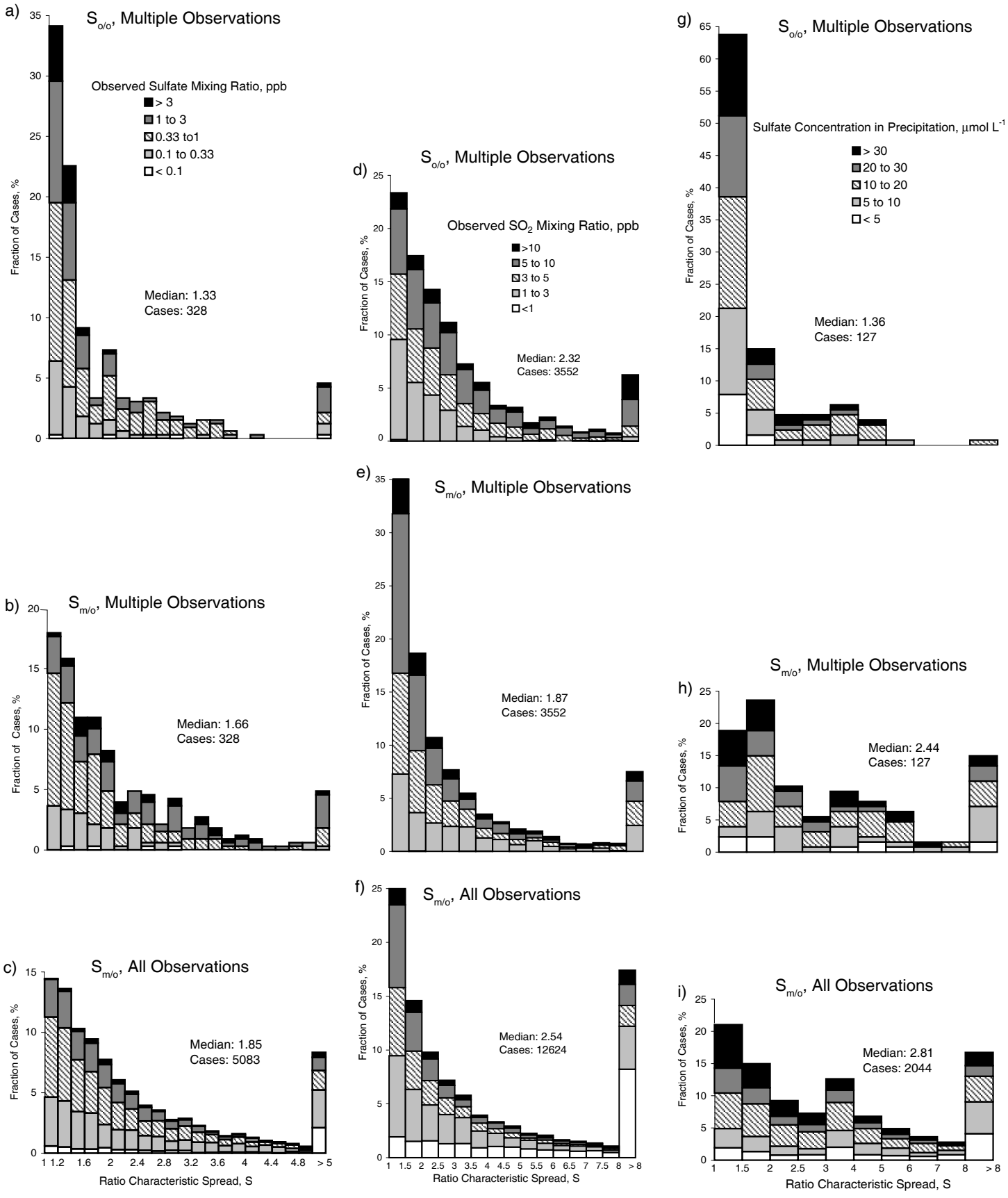
a)
$S_{o/o}$, Multiple Observations
Observed Sulfate Mixing Ratio, ppb
> 3
1 to 3
0.33 to1
0.1 to 0.33
< 0.1
Median: 1.33
Cases: 328
Fraction of Cases, %
b)
$S_{m/o}$, Multiple Observations
Median: 1.66
Cases: 328
c)
$S_{m/o}$, All Observations
Median: 1.85
Cases: 5083
1 1.2 1.6 2 2.4 2.8 3.2 3.6 4 4.4 4.8 > 5
Ratio Characteristic Spread, S
d)
$S_{o/o}$, Multiple Observations
Observed SO_2 Mixing Ratio, ppb
>10
5 to 10
3 to 5
1 to 3
<1
Median: 2.32
Cases: 3552
e)
$S_{m/o}$, Multiple Observations
Median: 1.87
Cases: 3552
f)
$S_{m/o}$, All Observations
Median: 2.54
Cases: 12624
1 1.5 2 2.5 3 3.5 4 4.5 5 5.5 6 6.5 7 7.5 8 > 8
Ratio Characteristic Spread, S
g)
$S_{o/o}$, Multiple Observations
Sulfate Concentration in Precipitation, µmol L^{-1}
> 30
20 to 30
10 to 20
5 to 10
< 5
Median: 1.36
Cases: 127
h)
$S_{m/o}$, Multiple Observations
Median: 2.44
Cases: 127
i)
$S_{m/o}$, All Observations
Median: 2.81
Cases: 2044
1 1.5 2 2.5 3 4 5 6 7 8 > 8
Ratio Characteristic Spread, S

Figure 11

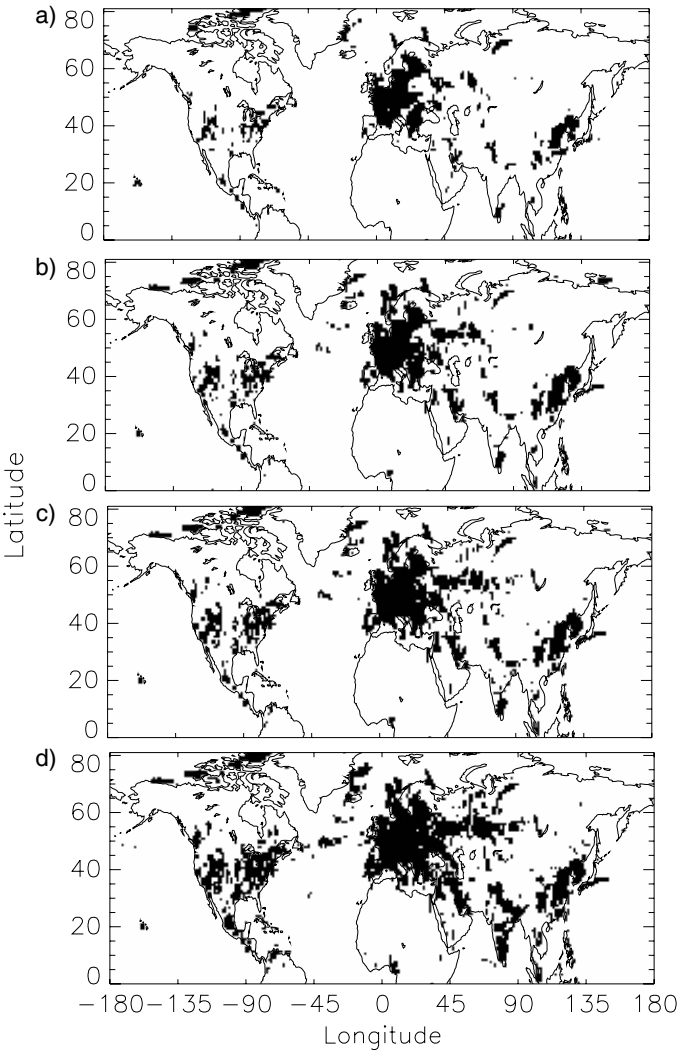
a)
b)
c)
d)
80
60
40
20
0
Latitude
−180 −135 −90 −45 0 45 90 135 180
Longitude

Figure C-1

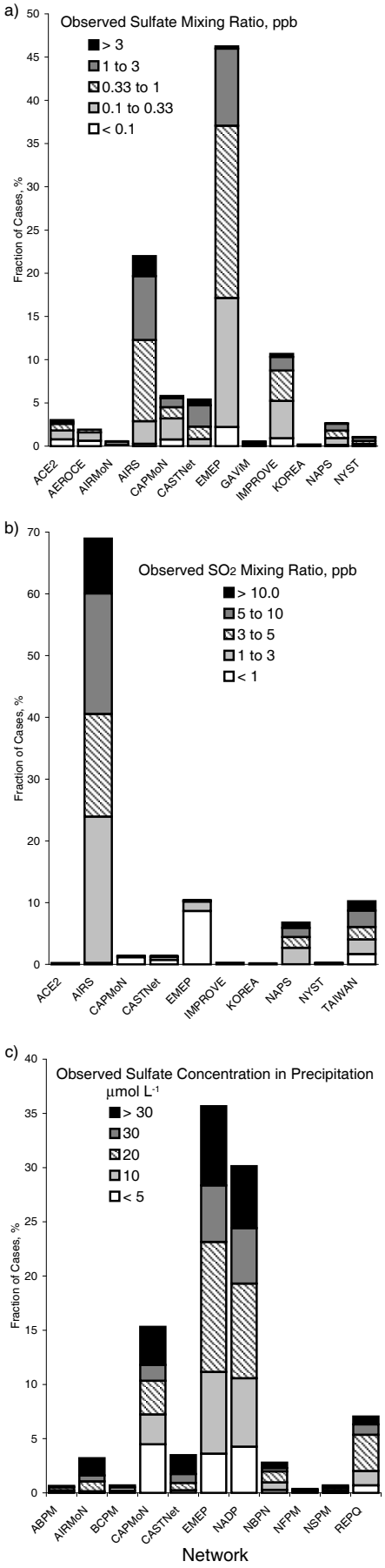
a)
Observed Sulfate Mixing Ratio, ppb
> 3
1 to 3
0.33 to 1
0.1 to 0.33
< 0.1
Fraction of Cases, %
ACE2
AEROCE
AIRMoN
AIRS
CAPMoN
CASTNet
EMEP
GAVIM
IMPROVE
KOREA
NAPS
NYST
b)
Observed SO2 Mixing Ratio, ppb
> 10.0
5 to 10
3 to 5
1 to 3
< 1
Fraction of Cases, %
ACE2
AIRS
CAPMoN
CASTNet
EMEP
IMPROVE
KOREA
NAPS
NYST
TAIWAN
c)
Observed Sulfate Concentration in Precipitation
µmol L-1
> 30
30
20
10
< 5
Fraction of Cases, %
ABPM
AIRMoN
BCPM
CAPMoN
CASTNet
EMEP
NADP
NBPN
NFPM
NSPM
REPQ
Network

Figure C-2

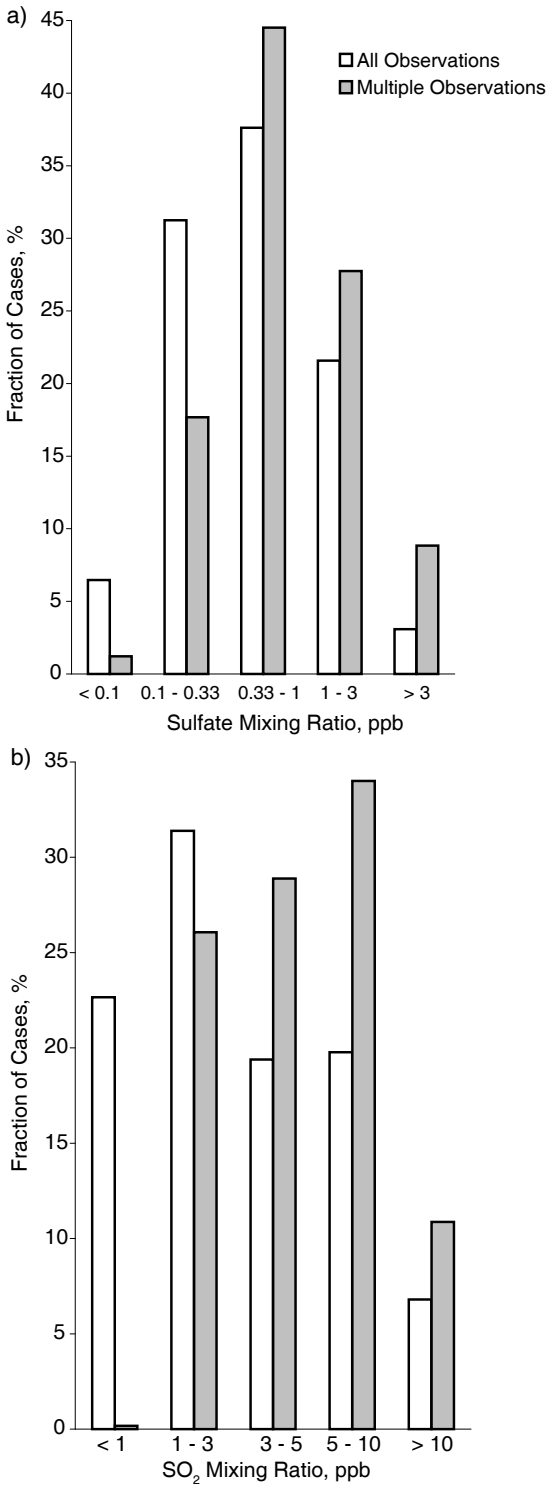
a)
All Observations
Multiple Observations
Fraction of Cases, %
0
5
10
15
20
25
30
35
40
45
< 0.1
0.1 - 0.33
0.33 - 1
1 - 3
> 3
Sulfate Mixing Ratio, ppb
b)
Fraction of Cases, %
0
5
10
15
20
25
30
35
< 1
1 - 3
3 - 5
5 - 10
> 10
SO2 Mixing Ratio, ppb